Gypsum, opal, and fluvial channels within a trough of Noctis Labyrinthus, Mars: Implications for aqueous activity during the Late Hesperian to Amazonian

Catherine M. Weitz [a,*], Janice L. Bishop [b], John A. Grant [c]

[a] Planetary Science Institute, 1700 E. Fort Lowell, Suite 106, Tucson, AZ 85719, United States
[b] SETI Institute, 189 Bernardo Ave., Mountain View, CA 94043, United States
[c] Center for Earth and Planetary Studies, National Air and Space Museum, Smithsonian Institution, 6th at Independence Ave. SW, Washington, DC 20560, United States

ABSTRACT

We investigate in detail the morphology, mineralogy, and stratigraphy of light-toned deposits within one trough of Noctis Labyrinthus, centered at $-6.8°$N, 261.1°E. CRISM spectra taken from light-toned layered deposits in the northern portion of the trough exhibit absorptions around 1.41, 1.92 and 2.21 μm, consistent with mixtures of opal and Al-clays that are exposed beneath younger lava flows and between high-standing mesas of chaotic terrain. In the southern portion of the trough, opal occurs as a patchy surficial deposit along the southwestern lower wall. Gypsum appears to be present in the southern portion of the trough where spectra show triplet absorptions at 1.44, 1.48, and 1.54 μm, and additional absorptions at 1.20, 1.74, 1.95, 2.22, 2.27, and 2.49 μm. The gypsum-bearing materials consist of one to several beds that typically fill low-lying regions, including valleys. A bright mound on the trough floor exhibits spectral features at 1.43, 1.92 and 2.43 μm, characteristic of polyhydrated sulfates. The bright mound appears distinct in morphology from chaotic terrain, and along its base are exposures of gypsum-bearing materials.

Fluvial channels in the southwestern portion of the trough incise surface slopes at 4–6° and lack obvious sources. The channels display first and second order tributaries arranged in a parallel pattern and may have formed by localized surface discharge from melting snow and/or ice. Both opal and gypsum occur in close proximity in the southwestern region of the trough, but gypsum is found alone in the southeast and opal in association with Al-clays is found to the northwest. We do not believe gypsum and opal formed coevally because they are not always found together, they require different aqueous conditions (i.e., opaline deposits require high silica availability while the gypsum deposits require high Ca availability in solution), and they appear at stratigraphically distinct levels. Although we identified evidence for fluvial landforms within the trough, cross-cutting relations indicate their incision post-dates deposition of the opal and pre-dates deposition of the gypsum. Hence, several periods of aqueous activity and alteration likely occurred within the trough from the Late Hesperian into the Amazonian that reflect favorable localized conditions within the Noctis Labyrinthus region and may be contemporaneous with late aqueous activity occurring elsewhere on Mars.

© 2013 Elsevier Ltd. All rights reserved.

1. Introduction

Hydrated minerals on Mars hold numerous clues into the environmental conditions that prevailed during water–rock interactions resulting in their emplacement. Recent and ongoing studies have placed important constraints on aqueous processes responsible for deposition of sediments in lacustrine systems or that have altered rocks by groundwater or surface flow. By identifying distinct mineral phases and determining how these minerals are associated spatially and temporally, it should be possible to decipher the changing nature of aqueous processes through time. Global observations of hydrated minerals of different ages suggest that ancient Mars was warmer and wetter, which favored formation of phyllosilicates, and through time changed to colder, drier conditions under which sulfates formed (Bibring et al., 2006). By contrast, Noctis Labyrinthus contains a diverse assemblage of minerals and landforms that suggest aqueous activity occurred relatively later. Sulfates and phyllosilicates identified within two depressions of Noctis Labyrinthus either resulted from localized aqueous activity (Weitz et al., 2011; Thollot et al., 2012) and/or may have been part of

* Corresponding author. Tel.: +1 571 766 0600.
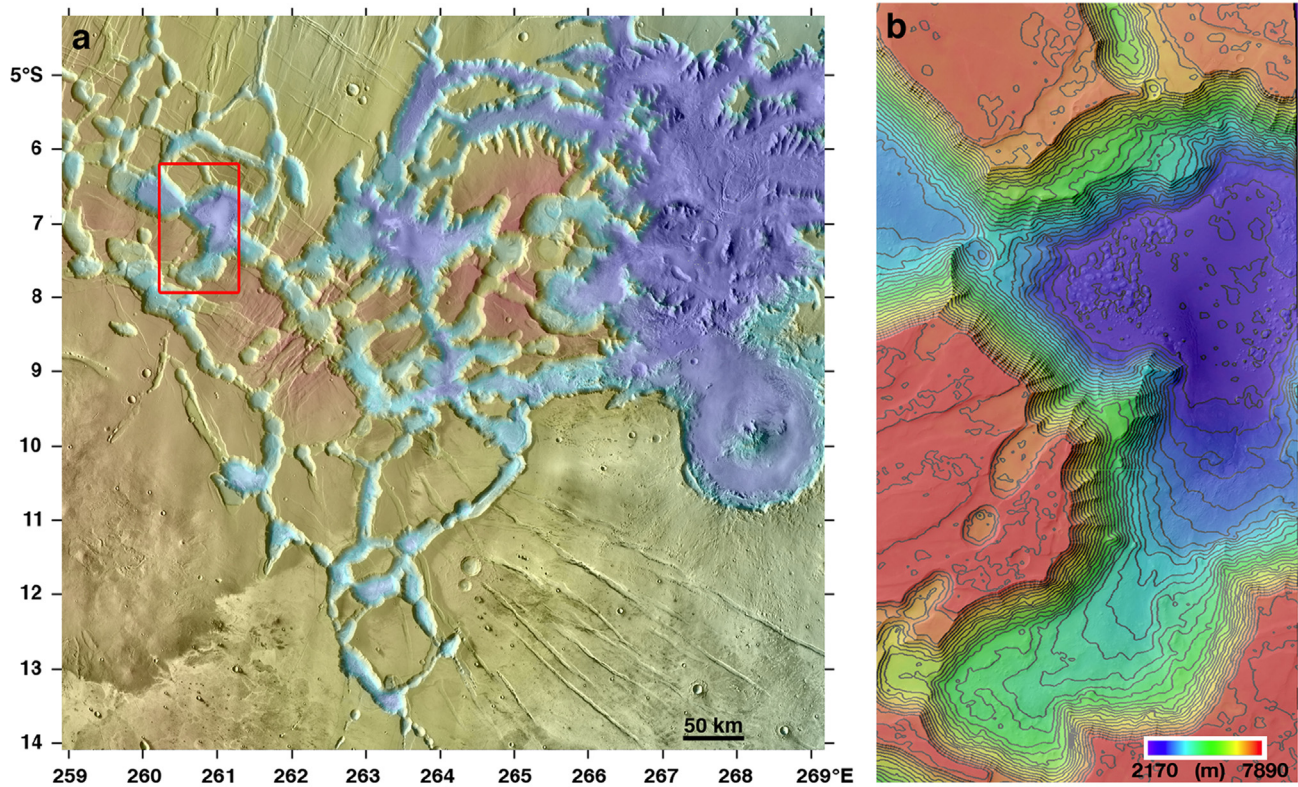 E-mail address: weitz@psi.edu (C.M. Weitz).

Fig. 1. THEMIS daytime IR mosaic with MOLA topography overlain in color for the Noctis Labyrinthus region. Red box shows location of blowup in (b). (b) HRSC DTM overlain on HRSC image 3155_0000_ND4 for the trough studied in this paper. Contours are marked at 200 m intervals and elevation values are for areoid reference. (For interpretation of the references to color in this figure legend, the reader is referred to the web version of this article).

a broader synoptically driven period of late activity (e.g., Grant and Wilson, 2011, 2012).

Noctis Labyrinthus, on the eastern edge of the Tharsis Plateau, consists of a network of intersecting valleys that merge and coalesce with pit chains and larger troughs (Fig. 1). Eastward, these depressions connect to the chasmata of Valles Marineris. The pits and troughs may have formed due to withdrawl of magmatic reservoirs at depth (Mège et al., 2003). The age of the Noctis Labyrinthus depressions is thought to be Late Hesperian to Early Amazonian based upon disruption of the lava plains along the plateaus (Scott and Tanaka, 1986; Tanaka and Davis, 1988). Consequently, sediments deposited within the depressions represent this age or younger materials. The larger interior layered deposits (ILDs) in the Valles Marineris chasmata typically consist of mixtures of polyhydrated and monohydrated sulfates (e.g., Murchie et al., 2009a; Bishop et al., 2009; Weitz et al., 2012). In contrast, regions along the plateau of Valles Marineris and in smaller depressions like those at Noctis Labyrinthus contain fewer sulfates and more hydrated silica and Fe/Mg-smectites (e.g., Milliken et al., 2008; Weitz et al., 2010, 2011; Le Deit et al., 2009, 2012).

This paper focuses on the spectral and stratigraphic analysis of aqueous minerals in a trough of Noctis that contains a diversity of minerals and sedimentary rocks. A major motivation of this study is to understand whether the sequence of deposits in this Noctis trough resulted from hydrothermal, lacustrine, or other aqueous settings. Emerging similarities or differences in inferred processes to form the deposits will be important for determining whether environmental effects were regional and similar across all of Valles Marineris or if they were localized in individual troughs of Noctis Labyrinthus.

The trough detailed in this paper is centered at $-6.8°$N, 261.1°E and is approximately 60×50 km in dimension with a depth of 5 km below the adjacent plateau (Fig. 1b). This location has been proposed as a future landing site on Mars due to a relatively flat
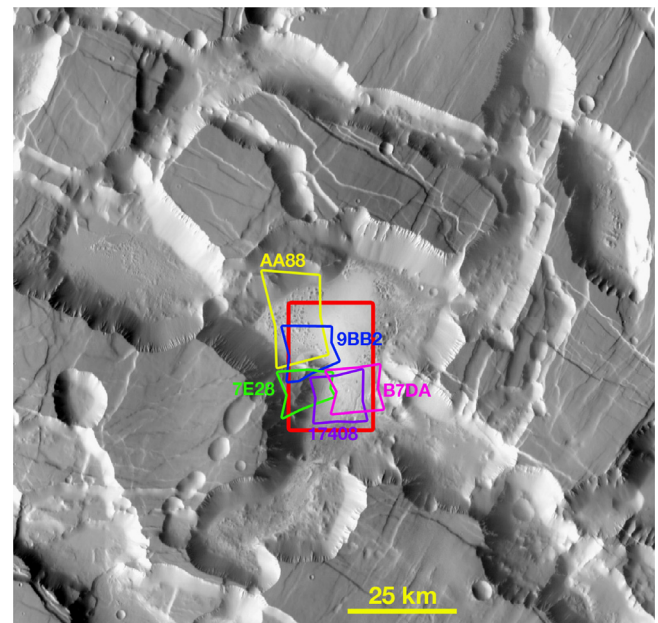

Fig. 2. THEMIS daytime IR mosaic of Noctis trough and surroundings. Red box indicates area of geologic map shown in Fig. 3 while other colors denote the locations of CRISM images analyzed in this study. Note the numerous linear troughs and pit chains that intersect the study trough. (For interpretation of the references to color in this figure legend, the reader is referred to the web version of this article).

region along the trough floor that could accommodate a MSL-class rover (20×25 km landing ellipse size, Grant et al., 2010), and also a diversity of hydrated minerals identified from orbit within the trough (Weitz and Bishop, 2011). Because this region was targeted

as a potential landing site, a wealth of data covers the deposits within the trough. Fissure vents and hummocky lava flows are visible across much of the trough floor in HiRISE images (Weitz and Bishop, 2011), with the age of these lava flows thought to be Late Amazonian (50–100 My old) (Mangold et al., 2010a). A pyroxene-rich mineralogy was deduced from OMEGA spectra by Mangold et al. (2010a), who interpreted the trough floor to be a lava plain covering an area of ~450 km². The trough is connected to several adjacent shallower troughs and pits (Fig. 2). For this paper, we divide the trough into northern and southern regions due to the distinguished geologic units and inferred history.

1.1. Data sets

We employed several Martian data sets representing a range of spatial and spectral resolutions, including the Mars Global Surveyor Mars Orbiter Laser Altimeter (MOLA, Zuber et al., 1992), Mars Odyssey Thermal Emission Imaging System (THEMIS, Christensen and Ruff, 2004), Mars Express High Resolution Stereo Imager (HRSC, Jaumann et al., 2007), Mars Reconnaissance Orbiter (MRO) High Resolution Imaging Science Experiment (HiRISE, McEwen et al., 2007), MRO Compact Reconnaissance Imaging Spectrometer for Mars (CRISM, Murchie et al., 2007), and MRO Context Imager (CTX, Malin et al., 2007). HiRISE images of 26 to 52 cm/pixel scales combined with lower-resolution CTX, HRSC, and THEMIS data were used to establish the juxtaposition of landforms and stratal geometries that, with compositional data from CRISM, record the geologic evolution of the surface. The large

swath sizes of CTX (30 km), THEMIS VIS (18 km), and HRSC (52.2 km at periapsis) coupled with their resolutions (6–20 m/pixel) enabled us to provide important local context and connectivity to individual HiRISE and CRISM observations. MOLA data (128 ppd global maps) were used to assist in stratigraphic placement, along with stereo anaglyphs from CTX and HiRISE for relative topography, and HRSC and HiRISE Digital Terrain Models (DTMs) for quantitative elevations (within the error associated with those data) and to help understand superposition and embayment relationships between geologic units.

Targeted observations by the CRISM instrument were acquired at 18 m/pixel spatial resolution (Full Resolution Targets, FRT) or 36 m/pixel spatial resolution (Half Resolution Targets, HRL). CRISM collects ~10-km-wide images from 0.4 to 3.9 μm over 544 channels (Murchie et al., 2007). Typical analyses of CRISM involved radiometric corrections (e.g., correction for the solar irradiance and geometry), atmospheric correction, and band parameterization and mapping (Murchie et al., 2009b). Radiometric correction is performed using a pipeline procedure that has been developed for the instrument. Atmospheric contributions are minimized using a scaled atmospheric template derived from observations of Olympus Mons (Murchie et al., 2009b). Finally, maps corresponding to diagnostic mineralogies were generated using spectral parameters developed by the CRISM team to map the distribution of minerals such as clays, sulfates, pyroxenes, and olivines (Pelkey et al., 2007; Murchie et al., 2009b).

We analyzed TRR3 images (calibration level 3) which include a more robust flat field correction, a correction for the effects of unremoved water vapor in observations of the ground calibration source to which inflight radiometric calibration is traced, and
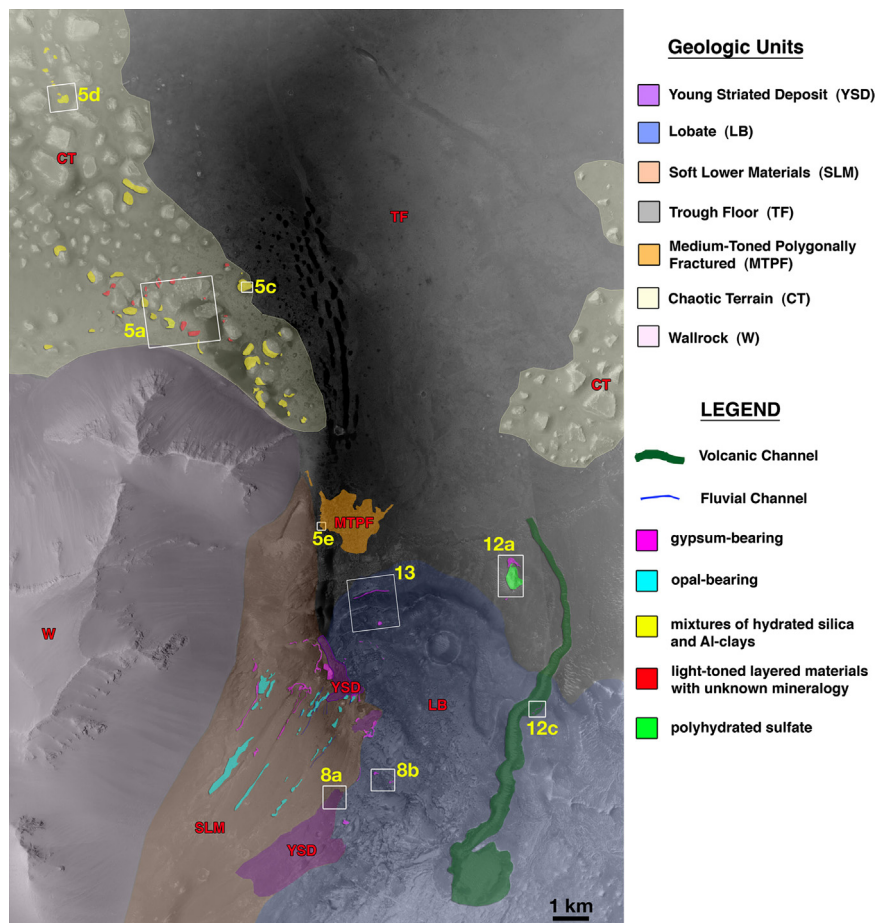

Fig. 3. Geologic map of units and features within the trough. Geologic units and mineral deposits are ordered in relative age, with youngest at the top. White boxes with numbers indicate locations of later figures. Mosaic of CTX images P15_007101_1740 and P15_006890_1717.

corrections for the effects of slight observation-to-observation irreproducibility in the viewing geometry of the inflight calibration reference (Seelos, 2011). Corrected *I/F* spectra were averaged into at least 3×3 pixel or larger regions of interest that showed common spectral features. All spectra were plotted as ratioed *I/F* values, where each spectrum of interest is divided by a denominator spectrum of a spectrally neutral region extracted from the same column(s) as the spectrum of interest to account for column-dependent systematic errors (Murchie et al., 2007, 2009b). Analysis of spectral features was performed by comparing the data to laboratory spectra of pure minerals for potential matches and through knowledge of the expected features and how their character varies with composition. In some cases difficulties associated with finding a perfect match to laboratory spectra can be attributed to subpixel mixing in the CRISM data, in which case plausible mineral mixtures are identified.

HiRISE images show morphology and derived stereo anaglyphs enabled stratigraphic relationships to be deciphered. Color HiRISE products were also utilized and include enhanced RGB and IRB images (McEwen et al., 2007). The freely available Integrated Software for Imagers and Spectrometers image processing routines (http://isis.astrogeology.usgs.gov) and the commercial SOCET Set image analysis software (http://www.socetset.com) were used to process one pair of HiRISE stereo observations into a DTM with elevation postings at every 1 m (Kirk et al., 2008). A HRSC DTM (Jaumann et al., 2007) that covered most of the trough was utilized as well (Fig. 1b). We used Orion structural analysis software to measure strike and dips along bedding exposures in the DTMs, and

employed the same restrictions as those by Okubo et al. (2008), including excluding measurements where the dip error is greater than the dip angle, or the dip direction error is greater than 30°, or the goodness of fit was less than 95%.

We define and map geologic units based upon morphology, which includes brightness. Because the brightness of any unit is subjective, the term "light-, medium-, and dark-toned" do not refer to a specific albedo range but rather to a unit's reflectance relative to other units within the same HiRISE image. In order to correlate mineralogy to morphology, CRISM spectral parameter color maps were registered to HiRISE images. All images are shown with north at the top unless noted otherwise.

2. Results

2.1. Northern floor

2.1.1. Chaotic terrain and trough floor

Along the northwestern portion of the trough (Figs. 3 and 4), there are numerous mesas and rocky mounds that comprise chaotic terrain (CT). The mesa tops are tilted and sloped, consistent with chaotic terrain seen elsewhere on Mars. Most mesas appear blocky and hummocky and lack obvious layering and spectral features in CRISM data. A dark mantle covers most of the mesa surfaces except where steep and rugged terrain exists. The chaotic material seen elsewhere along the trough floor (TF) appears to be covered by more dust and/or eolian debris, which
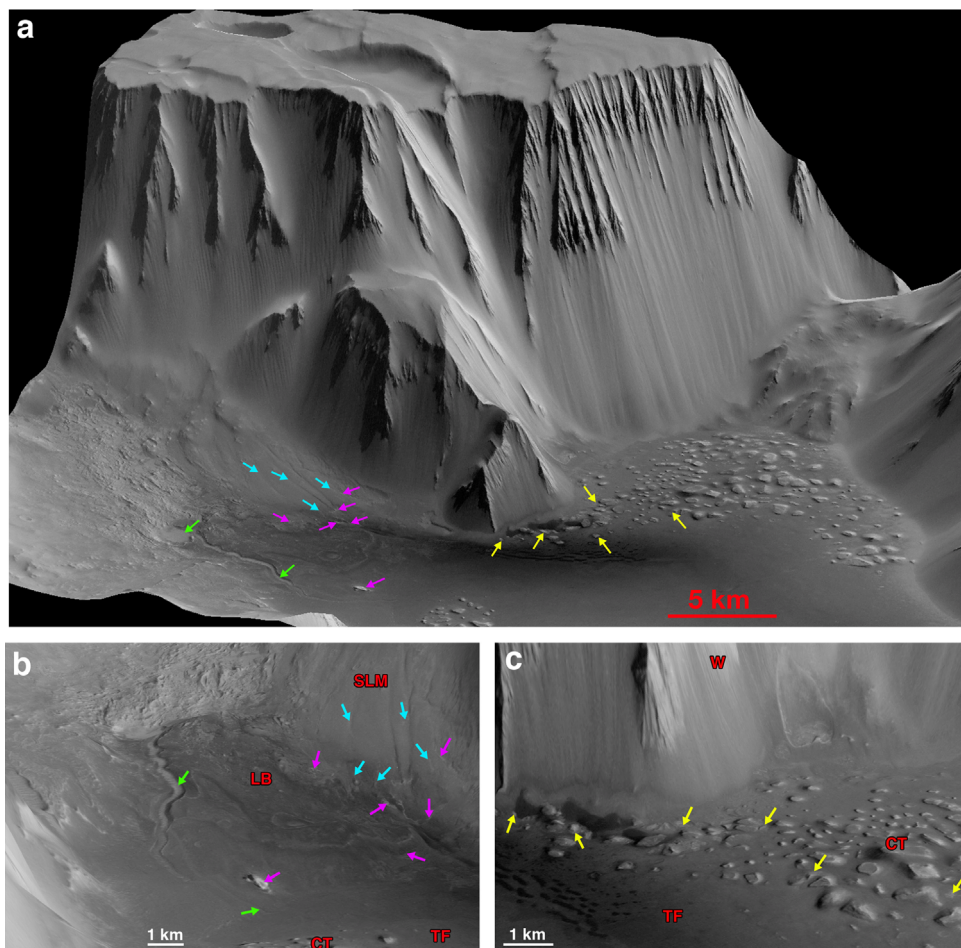

Fig. 4. (a) HRSC DTM perspective view looking west with 5X vertical exaggeration. Examples of gypsum (magenta arrows), opal (cyan arrows), mixtures of opal and Al-clays in the northern portion of the trough (yellow arrows), and a large channel (green arrows) are noted. DTM blowups showing the (b) southern and (c) northern portions of the trough at 10X vertical exaggeration. (For interpretation of the references to color in this figure legend, the reader is referred to the web version of this article).

may explain why no light-toned or layered material is visible within these mesas. Large dark sand dunes and eolian debris cover the central portion of the floor. At ~2 km below the plateau, there is a break in slope along the wallrock (W) that appears to coincide with the original floor of the trough, that was later lowered by additional collapse and widening to the current floor depth (Fig. 1b).

2.1.2. Light-toned layered deposits

Beneath several of the mesas in the northwest part of the trough and exposed between them are light-toned, sometimes layered, deposits (LTL) (Fig. 5). Most of the layering can be traced laterally across exposures, but some outcrops exhibit fracturing and faulting (Fig. 5c), suggesting disruption, perhaps due to later collapse within the trough. Layers vary from sub-meter to several meters thick, and brightness and color variations visible in HiRISE images suggest compositional differences.

CRISM spectra extracted from several of the layered deposits are consistent with Al-plyllosilicates and/or hydrated silica (Fig. 6a). Spectral absorptions for hydrated silica occur at 1.38–1.46, ~1.92, and 2.20–2.26 μm, which vary depending upon the hydration state, form and composition of the material, with opal representing one form of $SiO_2 \cdot nH_2O$ (Anderson and Wickersheim, 1964; Milliken et al., 2008). Related nanophase hydrated alluminosilicates such as allophane and imogolite exhibit similar features that vary depending on the degree of hydration and the Al/Si ratio (Bishop et al., 2013). Al-rich phyllosilicates exhibit Al–OH stretch+bend combination bands near 2.2 μm, while these bands are observed near 2.29–2.31, 2.33–2.34 and 2.35–2.37 μm for Fe^{3+}-rich, Mg-rich, and Fe^{2+}-rich phyllosilicates, respectively (e.g. Bishop et al., 2008). CRISM spectra exhibit features consistent with Al-rich phyllosilicates due to the presence of absorptions around 1.41 and 1.92 μm and a V-shaped 2.21 μm band. However, there is a reflectance maximum near 2.32 μm that is more consistent with opal than Al-clays (Fig. 6a). Other spectra display broader absorptions around 2.21 μm, also more characteristic of opal. Thus, opal is most consistent with the observed spectra, although mixtures of opal and Al-phyllosilicates are possible for some occurrences.

HiRISE images show bedding occurs at scales smaller than can be resolved in CRISM pixels so it is plausible that several mineral phases occurring in multiple layers may be mixed within any given CRISM spectrum. Additional mineral phases may be present, but they don't exhibit spectral features in the CRISM data because they occur in amounts too small to be detected. Other layered or light-toned units lack spectral features that might enable identification of a diagnostic mineralogy.

Based upon stratigraphic relationships interpreted from a HiRISE stereo anaglyph (Fig. 5b), the layered and light-toned material are interpreted to represent relatively older sediments deposited within the trough. Younger lava flows covered much of
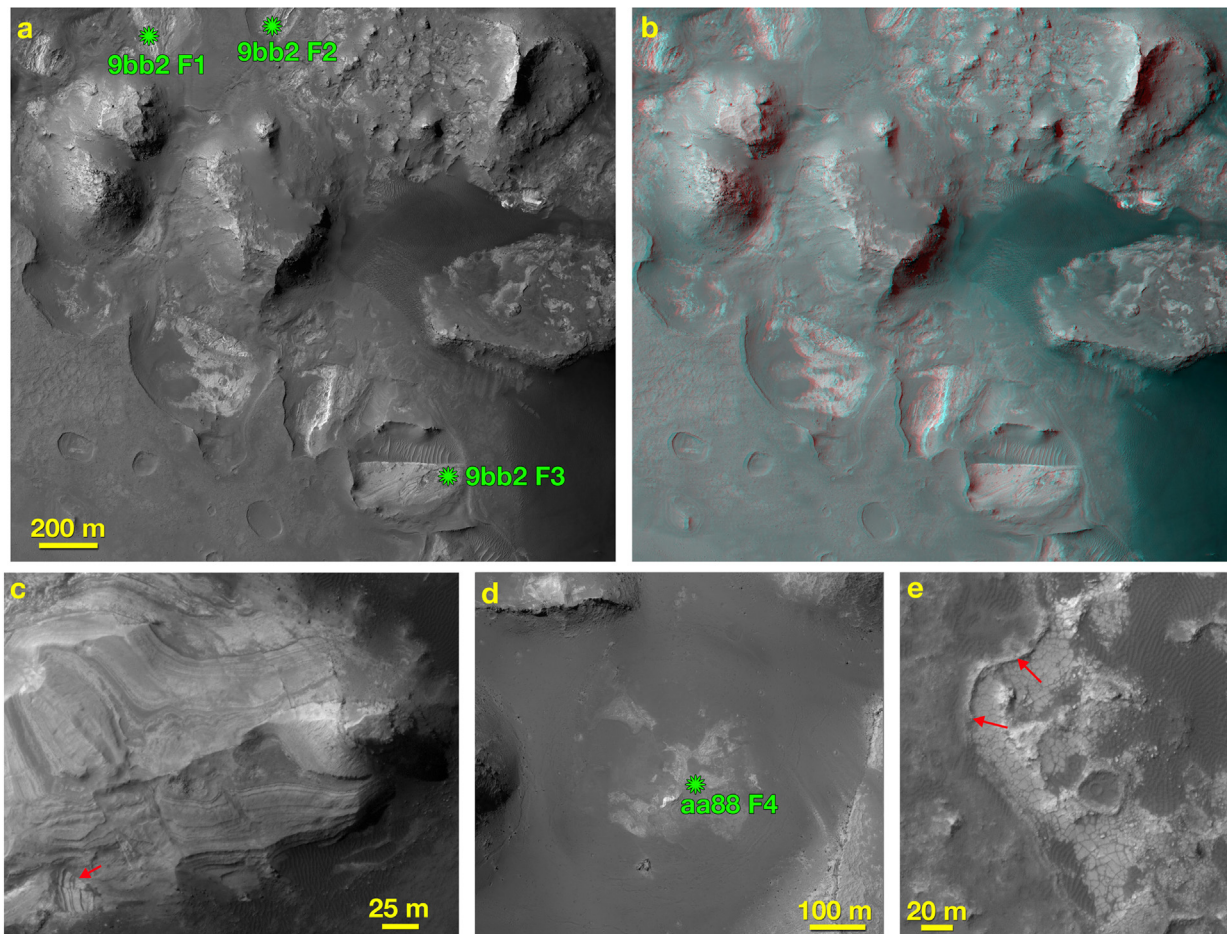

Fig. 5. Examples of deposits in the northern trough floor. (a) Portion of HiRISE image PSP_007101_1730 showing light-toned layered materials exposed around chaotic blocky mesas. Three locations where CRISM spectra were extracted (see Fig. 6) are shown by green asterisks and labels. (b) HiRISE stereo anaglyph showing the same area in (a). The light-toned hydrated materials are at lower elevations where the overlying lava flows have been removed by erosion. (c) Blowup of light-toned layered material with example of faulting indicating by red arrow. Portion of HiRISE image ESP_017610_1730. (d) Exposure of heterogeneous material that contains opal and Al-clays nestled between mesas of chaotic terrain. Location where CRISM spectrum was extracted (see Fig. 6) is shown by green asterisk and label. Portion of HiRISE image PSP_008393_1730. (e) Light-toned polygonally fractured material in unit MTPF. The contact between the underlying MTPF and overlying darker lava flows is identified by the red arrows. Portion of HiRISE image ESP_016120_1730. (For interpretation of the references to color in this figure legend, the reader is referred to the web version of this article).
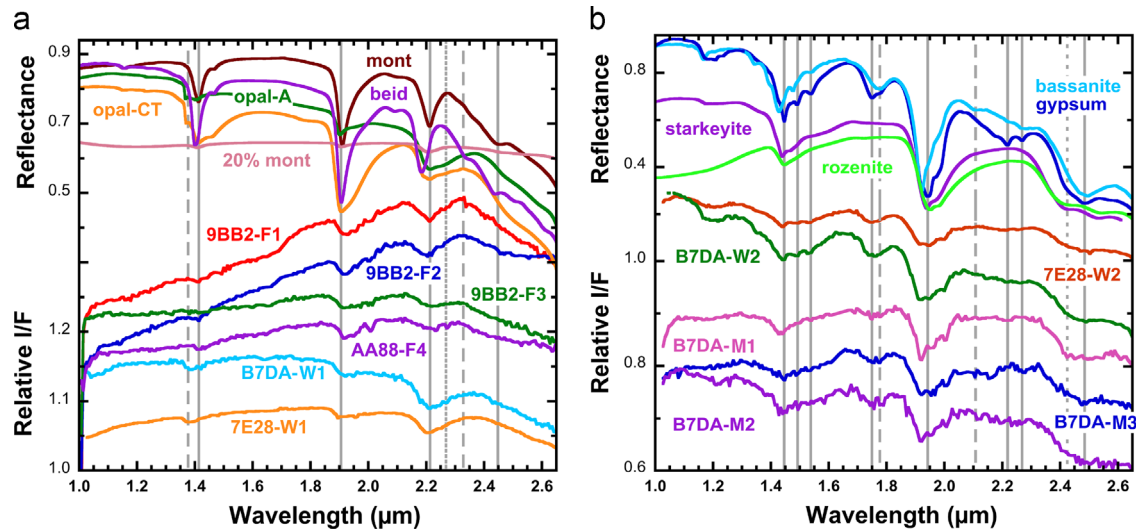
Fig. 6. Selected CRISM spectra of deposits in the trough. Some spectra have been offset for clarity. (a) Spectra of Si/Al-bearing deposits exhibiting absorptions at ~1.38–1.42, ~1.92 and ~2.18–2.21 μm. Laboratory spectra of opal-A, opal-CT, montmorillonite (mont), a montmorillonite/obsidian mixture (20% mont), and beidellite (beid) from previous studies (Bishop et al., 2008, 2011; McKeown et al., 2011) are shown for comparison. The montmorillonite and beidellite spectra are offset by +0.05. A reflectance peak at 2.32 μm is consistent with opal rather than montmorillonite. Labels indicate the CRISM image ID and the geologic feature where each spectrum was extracted, where F is trough floor and W is wall (see other figures for locations of spectra). (b) Spectra of gypsum-bearing deposits in the southern portion of the trough. Laboratory spectra of gypsum, bassanite, and two polyhydrated sulfates (starkeyite and rozenite) are shown for comparison. The starkeyite spectrum is offset by −0.2. Labels indicate the CRISM image ID and the geologic feature where each spectrum was extracted, where M is mound, and W is wall (see other figures for locations of spectra).
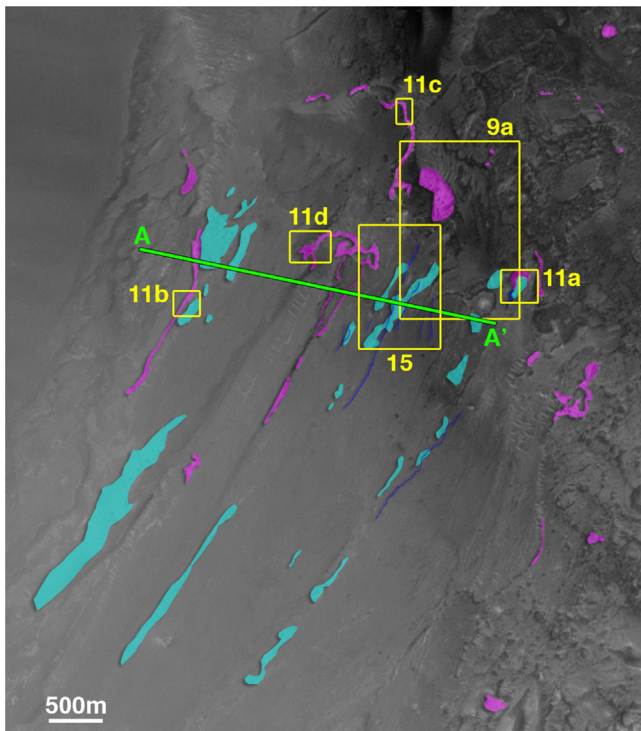

Fig. 7. Expanded view of the southwestern trough where there are numerous exposures of gypsum (magenta) and opal (cyan). Channels are mapped in dark blue. Green line is where the topographic profile in Fig. 14 was extracted. Yellow boxes and numbers indicate locations of later figures. Portion of CTX image P15_007101_1740. (For interpretation of the references to color in this figure legend, the reader is referred to the web version of this article).

the trough floor, burying the light-toned layered materials and embaying the mesas. Erosion of the lava flows in some locations later exhumed the light-toned layered material. Based on the occurrence and orientation of the LTLs, the deposit is likely to be more extensive at depth than the limited exposures seen along the surface.

2.1.3. Medium-toned polygonally fractured unit

A medium-toned polygonally fractured unit (MTPF) occurs further south. Superposition relationships reveal the lava flows are on top of MTPF (Fig. 5e). The size of polygonal fracturing in the MTPF varies from meter to tens of meters in diameter, and has created meter-size blocks that now rest upon the surface. The lighter reflectance and polygonal fracturing are uncharacteristic of lava flows but are morphologically similar to what is seen in association with hydrated units on Mars. CRISM spectra show no diagnostic features or hydrated signatures associated with this material, however.

2.2. Southern floor

2.2.1. Soft lower materials

In the southwestern portion of the trough, additional hydrated minerals can be found along lower wallrock slopes (Fig. 7). These hydrated minerals are associated with more easily eroded and presumably soft material near the lower slopes of wallrock (Soft Lower Materials, SLM). While slopes along the wallrock are ~28°, slopes on SLM are shallower, ~6°. We interpret the material to be low strength because eolian erosion has produced yardangs along a portion of the material, and both valleys and channels have dissected it. Collapse within the soft material reveals exposures ~20 m thick that show no evidence of layering or other morphologic heterogeneities. Otherwise, the surface of SLM is smooth where not punctuated by craters (Fig. 8), displaying an absence of boulders along the surface. Based upon these observations, SLM could be volcanic ash, eolian debris, and/or talus debris derived from upper wallrock slopes.

2.2.2. Lobate unit

We define a Lobate unit (LB) based upon occurrence of a lobate front that bounds the deposit near the trough floor. Unit LB is capped by a very rough surface displaying irregular shaped pits and mounds (Fig. 8). We interpret LB to represent a mass wasting lobe of material because the northern distal edge of the unit has a sharp rounded profile, consistent with a flow front. In addition, its
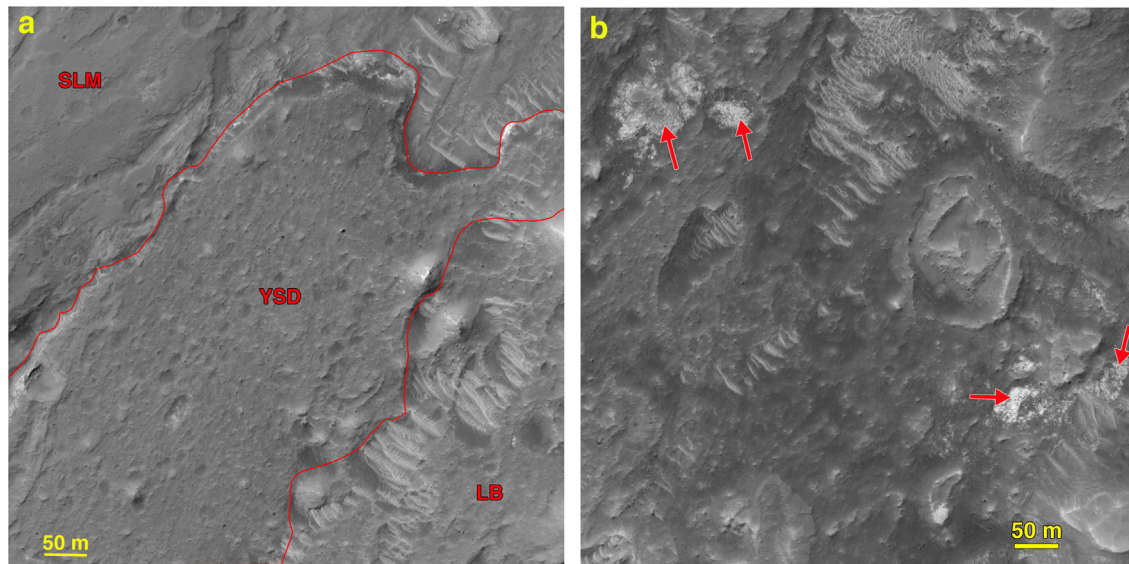
Fig. 8. (a) Portion of HiRISE image ESP_016120_1730 showing three units in the southern trough. SLM exhibits a smooth surface with channels. YSD appears rougher with boulders across the surface. The edge of YSD exhibits a sharp break in topography and reveals an underlying thin bright layer likely to be gypsum. LB is a rough disorganized unit with irregular pits and mounds, also shown in (b) where gypsum deposits are found in some of the pits (red arrows). (For interpretation of the references to color in this figure legend, the reader is referred to the web version of this article).

surface is disorganized and rough, also consistent with disruption experienced during a mass wasting event. Similar appearing deposits attributed to landslides and other mass wasting deposits are commonly seen within Noctis Labyrinthus troughs and Valles Marineris chasmata (McEwen, 1989; Quantin et al., 2004) and are likely enabled by steep slopes on bounding walls and the continued enlargement of these depressions over time.

2.2.3. Young striated deposit

We also define a differentially eroded dark-toned deposit, which we refer to as Young Striated Deposit (YSD). The HiRISE DTM shows the unit is a few meters thick and drapes across slopes ranging from 4 to 12°. Surface striations are seen on outcrops along steeper slopes and these appear to follow the topography, such as rounding around corners, suggesting they are related to flow that occurred in the deposit during emplacement. Downslope near the distal edge of the deposit, linear transverse ridges occur that are ~2–3 m high (Fig. 9). Backwasting has occurred along portions of YSD and the lower deposits appear separated from the upper deposit (Fig. 3). Meter-size blocks occur across the surface and there are small depressions that give it a rougher appearance than adjacent unit SLM (Fig. 8).

There are no morphologies diagnostic of emplacement process, and due to significant erosion, we are unable to decipher an origin for the YSD, although volcanic, mass wasting, and glacial appear to be the most plausible. Unit YSD appears to lie stratigraphically above units SLM and LB, as well as the gypsum and opal deposits (Fig. 9). In particular, along much of the base of YSD is a thin bright deposit that we suspect is gypsum based upon its morphology (see next section) even though most exposures are too small to be resolved in CRISM data.

2.2.4. Gypsum and other sulfate deposits

Numerous outcrops of relatively light-toned deposits occur throughout the southern portion of the trough (Fig. 10). CRISM spectra show the presence of both gypsum- and Si/Al-bearing materials. Features characteristic of gypsum include triplet absorptions at 1.44, 1.48, and 1.54 μm, and additional absorptions at 1.2, 1.74, 1.95, 2.22, 2.27, and 2.49 μm (Fig. 6b). If bassanite were present instead then we would expect similar absorption features, but at slightly different

wavelengths, and there should be an absence of absorptions at 2.22 and 2.27 μm (Wray et al., 2010). Other phases may be present with the gypsum but we map and refer to these rocks as gypsum because the spectral features are dominated by those associated with this mineral. CRISM spectra of opal are similar to those identified in the northwestern portion of the trough and include broad features around 1.38–1.42, 1.92, and 2.21 μm (Fig. 6a).

Where CRISM data was unavailable, we mapped additional exposures of both gypsum-bearing and Si/Al-bearing materials based upon analogous morphology and physical properties observed in CTX and HiRISE images. It is likely that both materials were once more extensive across the southern portion of the trough, but are now only preserved in areas where eolian erosion has not removed them. Exposures of gypsum along steeper slopes are partially covered by darker mass wasting materials, while flatter exposures are partially mantled by darker, likely eolian, debris. When mapping gypsum-bearing outcrops, lower lying terrain covered by darker debris was inferred to contain gypsum based upon the presence of adjacent high-standing gypsum exposures.

Along the base of the wallrock where unit SLM outcrops, the gypsum-bearing materials consist of several thin beds. Gypsum-bearing beds fill in low-lying regions, including valleys (Fig. 11a) and drape topography. For gypsum found on the SLM unit, bedding dips derived from the HiRISE DTM range from 5 to 11° towards the northeast, and are following the present surface slope of SLM. Based upon a HiRISE DTM where there was a vertical exposure through two beds within the gypsum unit (Fig. 11b), we estimate a thickness of ~5 m for each bed.

In HiRISE RGB images that cover the gypsum, white and orange beds can be interspersed (Fig. 11c). The orange beds have fractures at a greater scale than the white beds. The surface of the gypsum material is not smooth because small mounds appear in larger exposures, giving a bumpy appearance (Fig. 11d).

In the eastern portion of the trough is a bright mound that exhibits spectral features at 1.43, 1.92 and 2.43 μm, characteristic of polyhydrated sulfates (Figs. 6b, 12a; B7DA M1). Outcrops within this mound also include a possible absorption at 1.74 μm that could indicate the presence of gypsum-bearing materials as well. The mound appears distinct in morphology from the chaotic mounds along the trough floor because it has a higher reflectance and fracturing has created loose blocks along its surface. Lower lying portions of the mound are
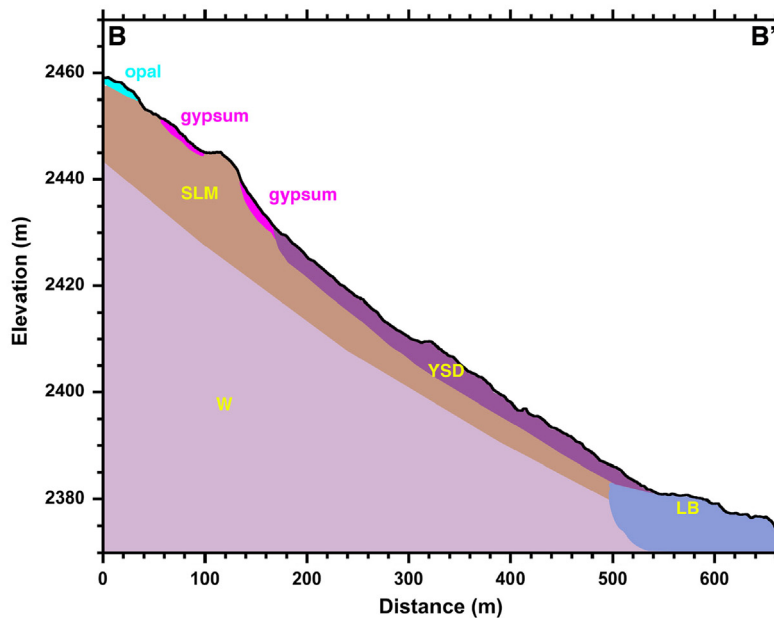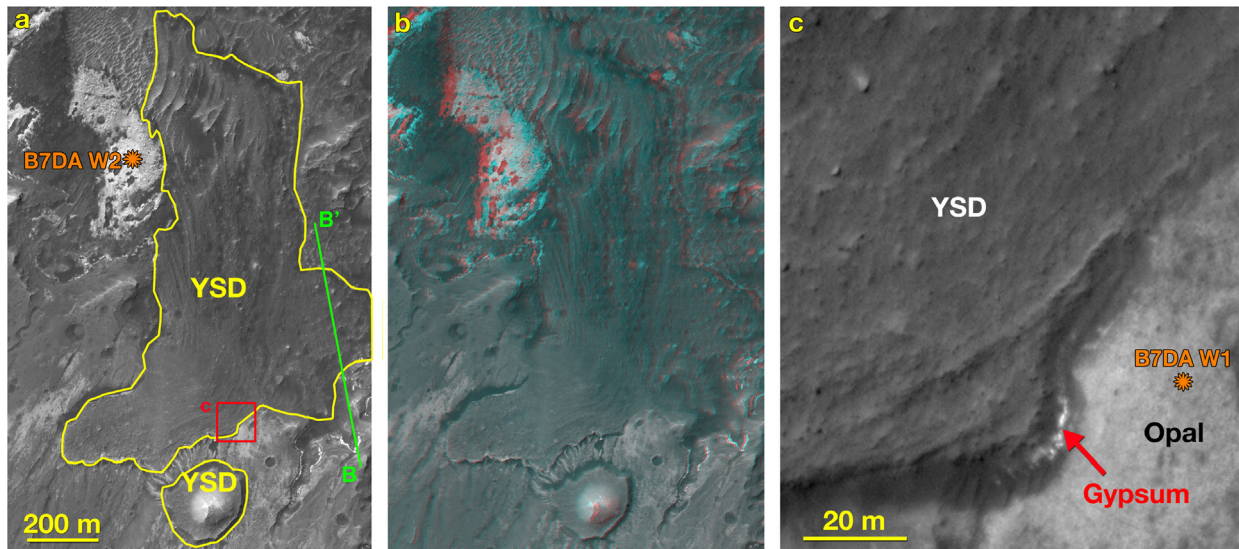
Fig. 9. (a) Example of unit Young Striated Deposit (YSD) seen in HiRISE image ESP_016120_1730. The red square identifies the location of blowup in (c) and the orange asterisk and label refer to the location where a CRISM spectrum was extracted (see Fig. 6b). Line BB' indicates the location of the topographic profile shown at the bottom, which illustrates approximated stratigraphic relationships and thicknesses of geologic units and minerals. (b) HiRISE stereo anaglyph showing the same area. Raised striations within YSD are visible at the top of the image. (c) Unit YSD appears to lie stratigraphically above gypsum and opal units. The orange asterisk and label refer to the location where a CRISM spectrum was extracted (see Fig. 6a). (For interpretation of the references to color in this figure legend, the reader is referred to the web version of this article).

mantled by dark debris while the upper surface has a thin veneer of light brown debris observed in enhanced HiRISE color images (Fig. 12a). Along and adjacent to the base of the mound are small patches of additional gypsum-bearing materials (Figs. 6b, 12a; B7DA M2, M3). The geologic contact between the gypsum-bearing patches and the polyhydrated sulfate mound is often partially obscured beneath dark debris, but where visible, the gypsum-bearing rocks appear to drape the polyhydrated sulfate rocks.

Several outcrops of gypsum occur in association with LB, generally seen filling in shallow pits and depressions along the LB upper surface (Figs. 8 and 13). Because the depressions do not exhibit raised rims or ejecta, we do not interpret them to be impact craters. One small patch of gypsum is located within a shallow depression on the surface of LB at an elevation of 2338 m (Fig. 13). A relatively thin bed of gypsum outcrops along the edge of LB at an elevation of ~2270 m where it occurs as a traceable

bed for up to ~1 km (Fig. 13). Below it are several other beds of unknown mineralogy and above it is the blocky and heterogeneous material of LB. Measurements from the DTM indicate the gypsum bed dips 6.4° towards the northwest, which is shallower than the ~12° surface slope measured along LB.

The gypsum bed could represent older material buried or perhaps transported by the mass wasting event that created LB, a deposit along a fracture or bedding plane, or a vein intruded within LB. If the gypsum both pre- and post-dates emplacement of LB then there must have been multiple episodes when gypsum was deposited. Gypsum commonly occurs on Earth in veins and has been found as veins at Endeavor crater, site of the Opportunity rover, albeit at much smaller scales (Squyres, 2012). If the gypsum bed seen in LB is a vein, then the processes responsible for its placement within the unconsolidated material of LB remain unknown. Another possibility is that the gypsum was transported
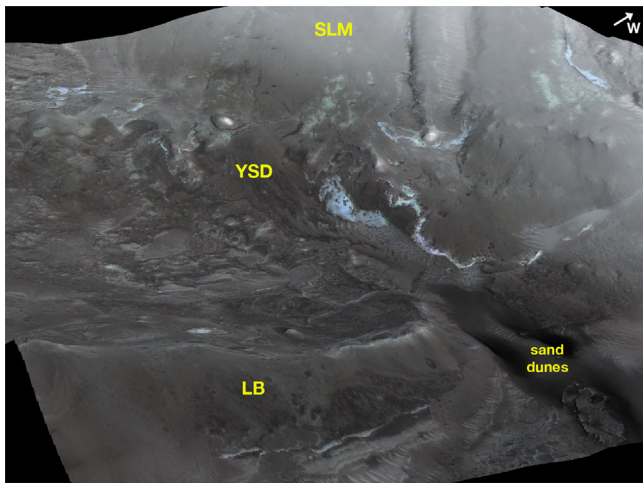
Fig. 10. HiRISE DTM perspective view of the southern trough area looking south-west with 5X vertical exaggeration. Colors from CRISM FRT00017408 (Red is 2.53 μm, Green is 1.51 μm, Blue is 1.08 μm) are overlain on the DTM, where light blue colors indicate the presence of gypsum and light green shows opal exposures. Note the gypsum bed within unit LB in the lower left. (For interpretation of the references to color in this figure legend, the reader is referred to the web version of this article).

along the base of LB as it moved downslope in a mass wasting event. Because the gypsum bed appears intact, this scenario seems unlikely, however. A third possibility is the gypsum was deposited along a fracture, fault, or bedding plane within LB, as observed in some terrestrial deposits (Kennedy, 1990; White and White, 2003).

2.2.5. Opal materials

Opal is only found as patchy outcrops on the surface of SLM. Its patchy appearance is likely due to variable degrees of erosion of a dark-toned eolian mantle overlying the opal that leads to only limited erosional windows that expose the deposit. Hence, the opal is probably more extensive across much of unit SLM but is only visible where erosion has removed the overlying eolian mantle.

Based upon stratigraphic relationships seen in HiRISE images (Fig. 11a, b), we interpret the opal as material beneath the gypsum. Because we cannot rule out the possibility that opal formed as an alteration product on SLM after erosion removed the overlying gypsum unit, the opal may be either younger or older than the gypsum deposit. However, we observe channels that dissect the opal material but are filled in by gypsum, which would favor a younger age for the gypsum-bearing material relative to the opal-rich material. Darker eolian debris and mass wasting material later covered much of the opal and gypsum materials.

2.2.6. Valleys and channels

Small channels and valleys dissect through unit SLM, including the opal deposits. Most channels are only 1–2 m deep and of a constant width ranging from 1 to 5 m wide based upon DTM measurements (Fig. 14), and display first and second order parallel drainage patterns. The channels are found only at lower elevations where surface slopes are 4–6°, and the absence of channels on higher surfaces implies the source of runoff, which we cannot ascertain, was distributed along the slopes rather than coming from basin-wide surfaces. As one channel approaches steeper slopes ($>10°$) the channel incises and the encompassing valley widens (Fig. 15). The low densities coupled with constant widths are consistent with incision related to point source discharge from fluvial flow as there is no lava at the terminus of them. Moreover, the constant width implies incision was related to sources upslope with little addition of discharge further downstream. Based upon these observations, we

interpret the channels to be sourced either from melting snow and/or ice that once mantled higher slopes, or from another unit that has since been eroded. However, given the good preservation of the channels, upstream erosion seems unlikely.

We only mapped (Figs. 3,7) channels with characteristic mean-der patterns consistent with water flow. Numerous other features along the wallrock could also be channels but they did not display meander patterns, and consequently, we could not rule out the possibility that these are related to fractures or trails left by rock falls or other mass wasting activity.

A larger ~30 m deep and ~9.5 km long sinuous channel occurs in the southeast part of the trough (Figs. 3 and 4) (Mangold et al., 2010a). There is a ~90 m deep and ~1 km diameter rounded pit at the source, and lava flows extend from the terminus of the channel. Hence, this channel is more consistent with a volcanic rather than fluvial origin. Using the HiRISE stereo anaglyph, the floor of the rounded pit can be seen below the floor of the channel, thereby indicating that not all lava drained from the pit via the channel. Both the pit and upper channel floors are covered by bright linear ripples and along one wall of the channel there are a few small outcrops of light-toned material (Fig. 12c, d). CRISM spectra extracted from these light-toned deposits are noisy due to their small outcrop sizes, but appear to be consistent with gypsum. In addition, their light-toned reflectance, draping across uneven surfaces, polygonal fracturing, and weathering into small blocks are similar to the physical properties of the gypsum deposits seen further west.

2.3. Discussion

On Earth, gypsum is a common sedimentary mineral found in evaporite beds (e.g. Prothero and Schwab, 2004). Gypsum is one of the first minerals precipitated from seawater of normal salinity because Ca^{2+} and SO_4^{2-} are less soluble than other ions. Thick, extensive gypsum deposits are less common, but are observed in shallow basin environments (e.g. Hardie and Eugster, 1971). Gypsum can also form by sulfuric acid solution or vapors through fumarole activity, and it is also found in ash and ejecta blocks (e.g. Belousov, 1995; Holland, 2002). Gypsum generally forms at temperatures below 60 °C (e.g. Conley and Bundy, 1958).

Hydrated silica deposits on Earth occur in active fumaroles where basaltic rocks and tephra undergo acid sulfate weathering (Morris, 2000; Bishop et al., 2005). Opal is a crystalline form of hydrated silica that can be sub-divided into opal-A, opal-CT, and opal-C depending upon the degree of aqueous alteration (Williams et al., 1985). Opal-A is associated with volcanic rocks and generally forms at temperatures below 100 °C and can convert to opal-CT during diagenesis (e.g. Elzea et al., 1994). Opal-A is thought to form subsequent to montmorillo-nite in volcanic ash via a mechanism involving hydrated silica (Henderson et al., 1971). Opal also forms in marine environments and mixed silica/montmorillonite systems could be indicative of submarine volcanism (e.g. Henderson et al., 1971; Calvert, 1974). Thus, the gypsum-rich and opal-rich materials forming in this trough could have formed under similar mildly acidic, low tem-perature conditions; however, the opaline deposits require high silica availability in solution, while the gypsum deposits require high Ca availability in solution.

Both gypsum and opal have been identified and analyzed in situ on Mars by the Mars Exploration Rovers. The Spirit rover detected hydrated silica in soils and outcrops adjacent to Home Plate in Gusev Crater (Squyres et al., 2008; Rice et al., 2010). The opal has been interpreted as evidence for hydrothermal activity, perhaps as a precipitate in a hot springs environment (Ruff et al., 2011). Gypsum has been found in veins at Endeavor Crater by the Opportunity rover (Squyres, 2012). The gypsum is interpreted to have formed as water flowed through cracks in the subsurface, dissolving out calcium and sulfur from the rocks that then com-
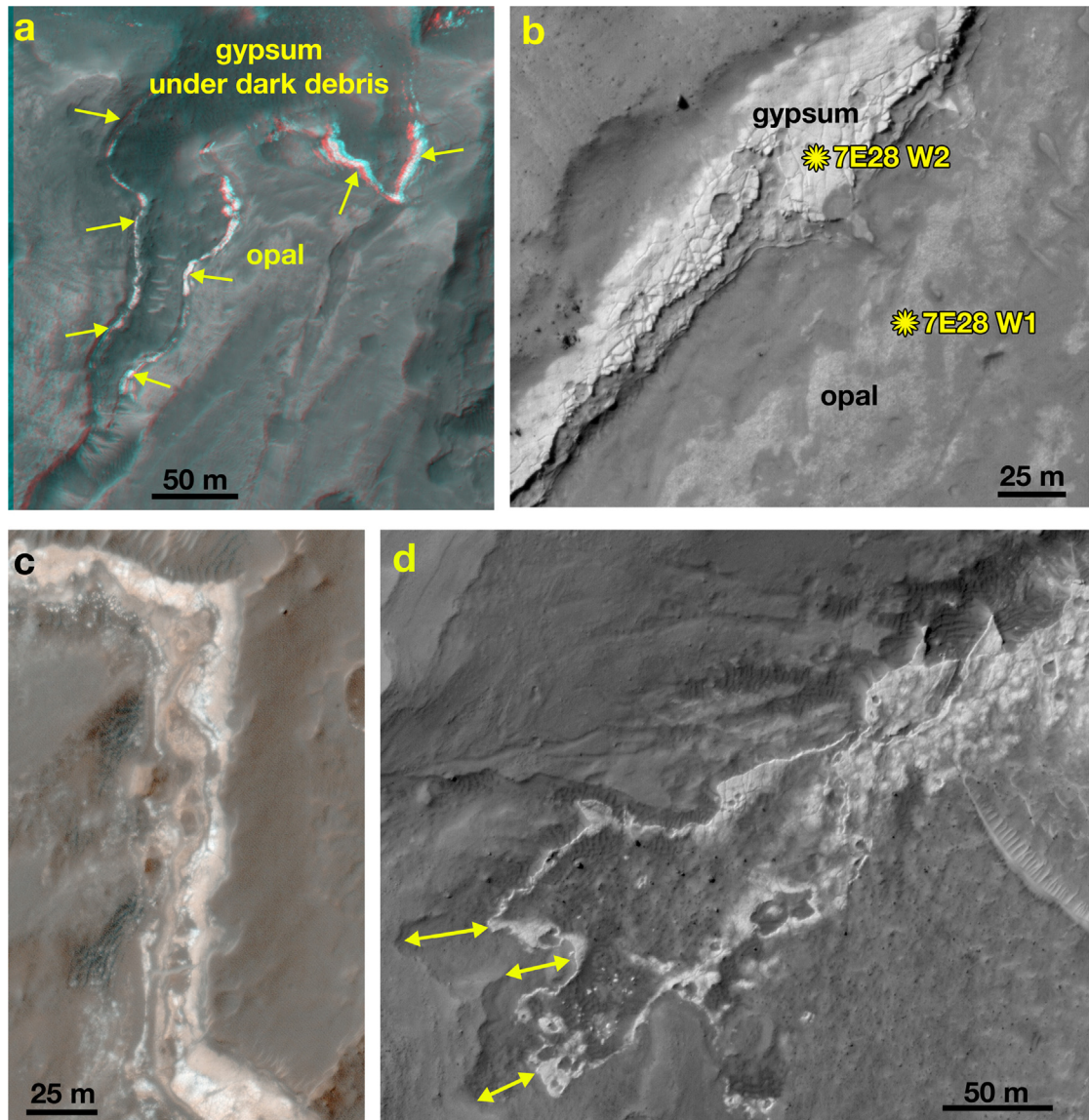
Fig. 11. Exposures of gypsum and opal in the southern portion of the study region as seen in HiRISE image ESP_016120_1730. (a) Portion of HiRISE stereo anaglyph. Gypsum occurs within a valley while opal is exposed outside the valley. The gypsum has bright edges at the higher elevations (arrows) but is buried beneath darker debris in lower portions of the valley. (b) Polygonal fracturing is visible in the gypsum material and at least two beds of gypsum are exposed. Stratigraphically below the gypsum beds are patches of opal. The yellow asterisks and labels refer to the locations where CRISM spectra were extracted (see Fig. 6). (c) HiRISE enhanced color illustrating diverse colors and lithologies visible in the gypsum-bearing rocks. (d) Bright gypsum material that has infilled a valley and lower elevations. The gypsum material exhibits a bumpy texture in this location. Yellow arrows identify where the edge of the gypsum-bearing rock matches the edge seen in the bedrock, suggesting the gypsum once extended to these higher elevations but has been subsequently removed by erosion. (For interpretation of the references to color in this figure legend, the reader is referred to the web version of this article).

bined to produce calcium sulfate. Later, these underground veins became exposed along the surface (Squyres, 2012). Gypsum has also been found in some rocks and soils of the Columbia Hills in Gusev crater (Squyres, 2006; Yen et al., 2008).

Orbital detections of gypsum have been studied in the north polar sand dunes on Mars using OMEGA (Langevin et al., 2005; Fishbaugh et al., 2007) and CRISM data (Masse et al., 2011). Fishbaugh et al. (2007) postulated the gypsum formed by water sourced from nearby channels percolating through the dunes, while Masse et al. (2011) suggested the gypsum crystals were originally present within the interior of the North Polar Cap and have collected as ablation tills by ice sublimation and then subsequently been reworked by winds. Masse et al. (2011) proposed the gypsum crystals within the polar car formed by weathering of dust particles. Szuimula et al. (2013) found that gypsum has a higher abundance in primary dunes rather than secondary

dunes, indicating that gypsum was likely present when the dunes formed and may be altering under current conditions.

Wray et al. (2010) used CRISM spectra to identify gypsum associated with Fe/Mg-sulfates in a discreet ring around the walls of Columbus crater (Wray et al., 2011) while Weitz et al. (2013) found gypsum in outcrops along the western Melas Chasma floor. Mangold et al. (2010b) noted that a Ca-sulfate in a separate Noctis trough farther to the east was unlikely to be an evaporitic deposit because the material appeared to be draped across multiple elevations and there was a lack of fluvial landforms. The favored model put forward by Mangold et al. (2010b) attributed formation of the Ca-sulfate to local frost/snow that interacted with sulfur from gas and/or rocks to alter the rocks into gypsum.

Hydrated silica is a mineral commonly identified in a range of locations on Mars (e.g., Milliken et al., 2008; Skok et al., 2010; Flahaut et al., 2010; Weitz et al., 2011) and has many varieties
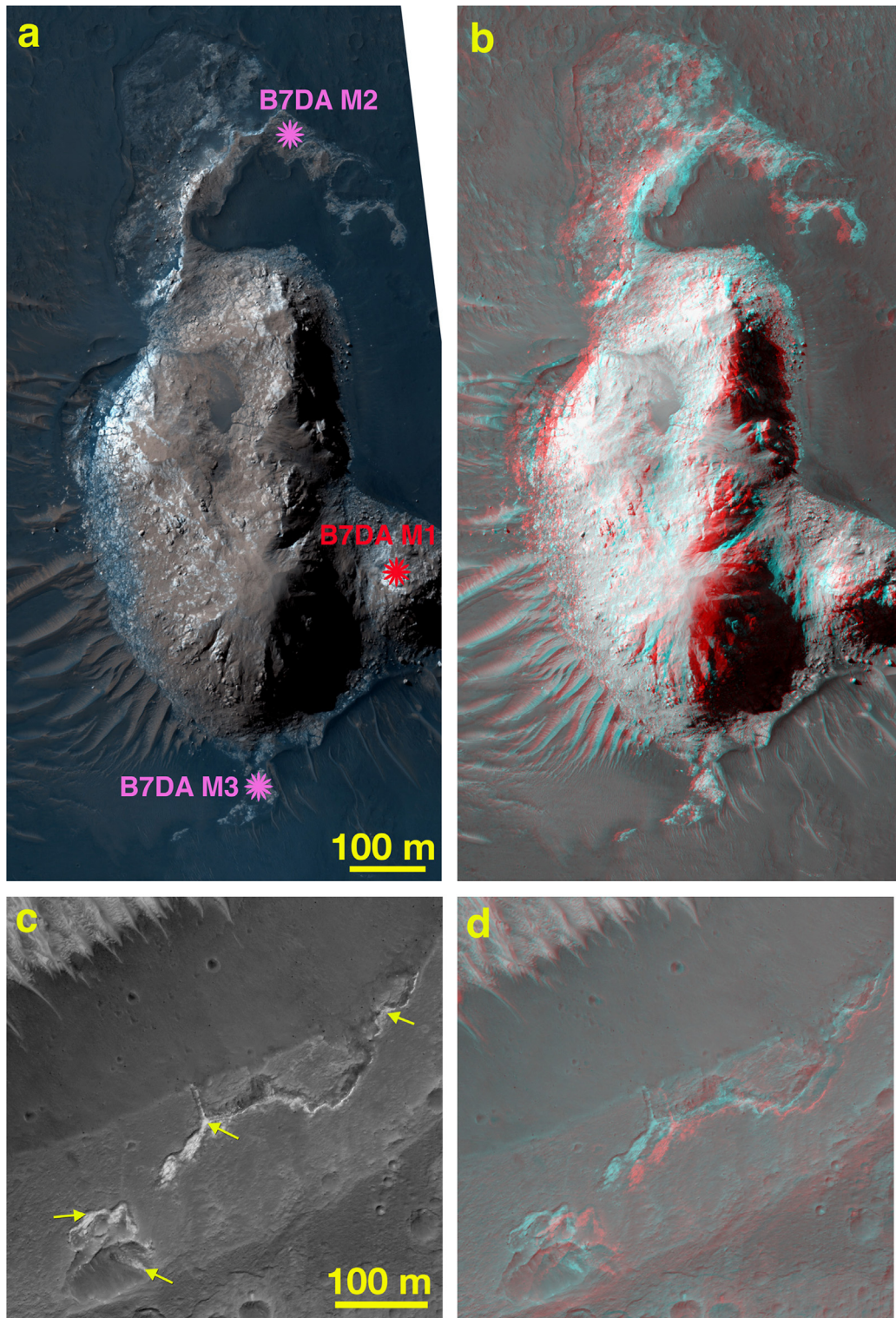
Fig. 12. (a) Mound with polyhydrated sulfates near the southern floor of the trough as seen in this enhanced color HiRISE image ESP_017966_1730. The colored asterisks and labels refer to locations where CRISM spectra were extracted (see Fig. 6). (b) HiRISE anaglyph of the same mound. (c) Channel wall with exposures of gypsum (yellow arrows). (d) HiRISE stereo anaglyph demonstrating how the gypsum is preserved only along depressions and edges within the channel wall. (For interpretation of the references to color in this figure legend, the reader is referred to the web version of this article).

depending upon the degree of crystallinity and water content. Studies have shown that minor aqueous alteration of silica-bearing rocks on Mars would liberate silica (McLennan, 2003), and this silica could later precipitate to form opal. Other troughs of Noctis Labyrinthus contain hydrated silica in association with monohydrated and polyhydrated sulfates, and in one trough with clays (Weitz et al., 2011; Thollot et al., 2012). These mineral associations are consistent with acid-leaching that would favor silica precipitation.

In this Noctis trough, both opal and gypsum are found in close proximity in only the southwestern region, while gypsum occurs alone in the southeast whereas opal is found in association with Al-phyllosilicates to the northwest. Gypsum and opal are not
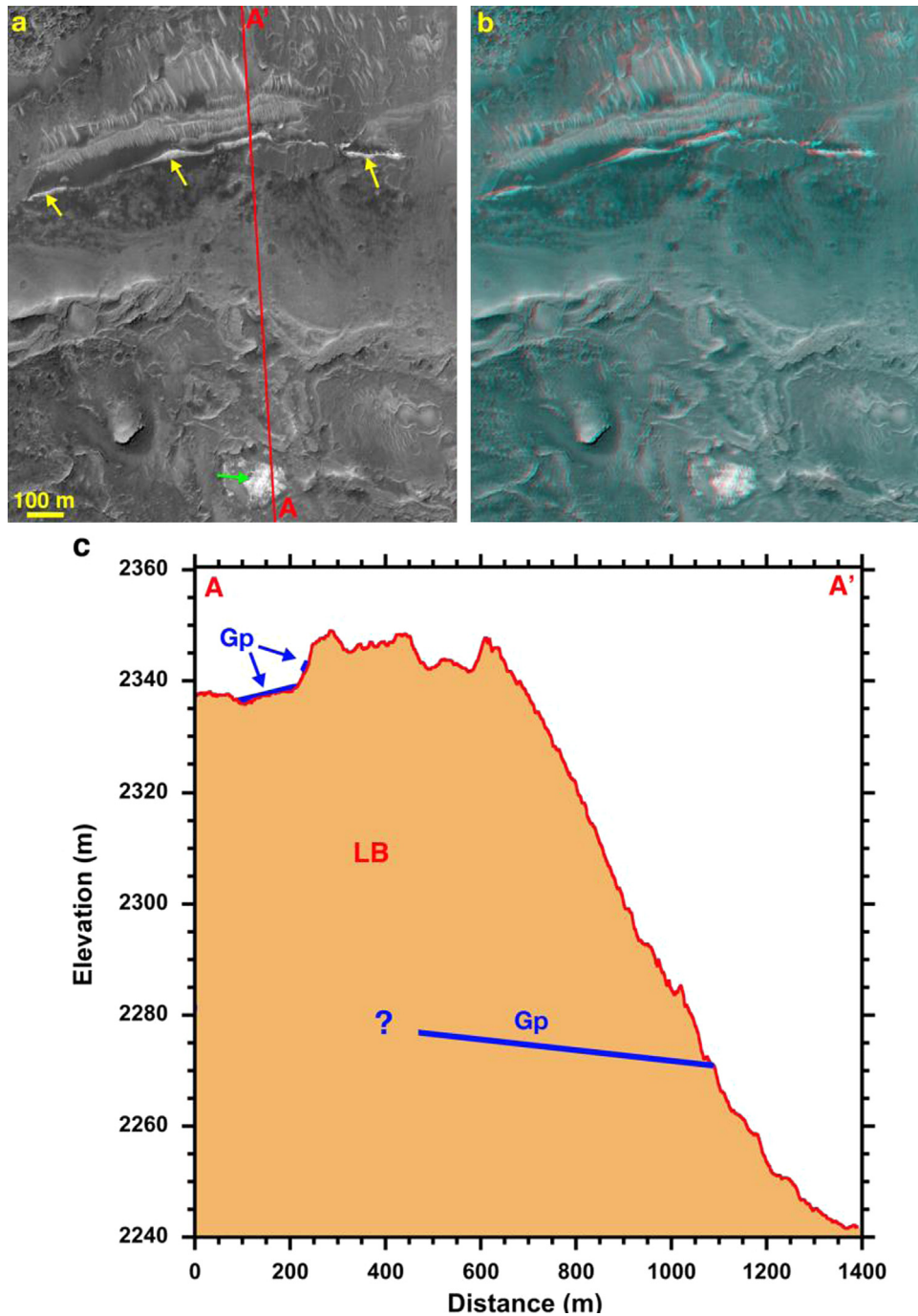
Fig. 13. (a) Gypsum (Gp) is found as a draping unit within a shallow depression on the surface of LB (green arrow) and also as a bed near the base of LB (yellow arrows) in this portion of HiRISE image ESP_017043_1730. Red line indicates location of topographic profile shown in (c). (b) Stereo anaglyph of same area shown in (a). (c) Topographic profile across the front edge of LB. The gypsum bed has a dip of 6.4° to the northwest and can be traced over 1 km in length. How far it extends within unit LB is unknown. (For interpretation of the references to color in this figure legend, the reader is referred to the web version of this article).

always found together because they generally require different water chemistry to form. Because they appear at stratigraphically distinct levels within the trough, we do not believe they formed coeval under the same conditions. The polyhydrated sulfate materials found in association with the mound along the southeastern portion of the trough could represent an earlier phase of aqueous deposition that has subsequently been eroded through time and buried by younger lava flows. Gypsum covers portions of this mound and could have formed at the same time as the other gypsum exposures in the trough.

The different colored beds associated with the gypsum deposit suggest changing environmental conditions during emplacement,

such as between conditions favoring anhydrite and gypsum, or other minerals undetectable by CRISM. Because the gypsum has not dehydrated to bassanite, conditions must have remained cold after gypsum formation and/or the gypsum consists of a coarser size fraction (Vaniman et al., 2008). Although the trough is located at an equatorial site where summer temperatures could be high enough to dehydrate gypsum, the elevation of the trough is 2 km above the datum where colder conditions exist. And while the pit that sourced the lava channel in the eastern portion of the trough may have emitted volcanic ash and gases, most of the opal and gypsum discussed herein is located several kms away. Without any evidence for volcanic vents nearer the opal and gypsum in the
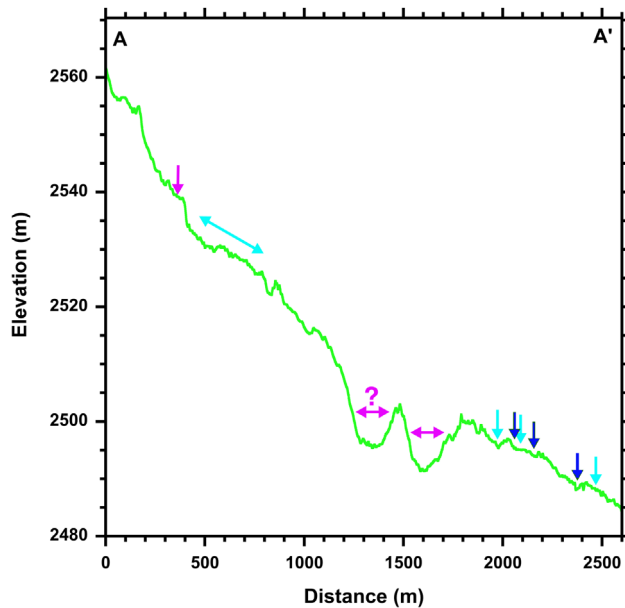
Fig. 14. Topographic profile derived from HiRISE DTM taken along line AA' shown in Fig. 7. Colored arrows correspond to features mapped in Fig. 7, including gypsum (magenta), opal (cyan), and channels (dark blue). (For interpretation of the references to color in this figure legend, the reader is referred to the web version of this article).

Fig. 15. Examples of fluvial channels (green arrows) in the southern portion of the trough as seen in this portion of HiRISE image ESP_017043_1730. Gypsum does not appear to be associated with the channels, while opal is dissected by the channels. The top green arrow shows where a channel broadens when the surface slope increases. (For interpretation of the references to color in this figure legend, the reader is referred to the web version of this article).

southwestern floor of the trough, an origin related to fumaroles remains uncertain.

Although we identified evidence for fluvial landforms within our study trough, cross-cutting relationships demonstrate that the opal pre-dates and the gypsum post-dates these channels, respectively, rather than being contemporaneous. Melting snow/ice could provide the water for precipitating opal by low-temperature aqueous alteration of rocks. If hydrothermal conditions existed that enabled snow and ice to melt, then the associated heat would also allow gypsum to precipitate. Acidic snow interacting with volcanic rocks or ash is another possibility, with the gypsum precipitating from this interaction where it could collect in channels and valleys. We note that both the gypsum and opal drape underlying topography and occur at multiple elevations, which is inconsistent with a lacustrine origin given the absence of other diagnostic landforms of such an environment. For the same reasons, an alteration sequence derived from ground-water and magmatic sulfur (Thollot et al., 2012) does not appear likely to explain all of the opal and gypsum deposits within this trough.

We interpret the opal-bearing units and other light-toned layered deposits in the northwestern portion of the trough to represent an older episode of alteration before emplacement of the lava flows during the Late Amazonian (Mangold et al., 2010a). The polyhydrated sulfate mound may represent an additional remnant of this early period of aqueous activity within the trough that was subsequently eroded and covered by lava flows, with only this high-standing mound still visible. In contrast, the opal and gypsum seen in the southern portion of the trough represents a younger period of alteration that post-dates emplacement of the trough lava flows based upon superposition relationships. Hence, several periods of aqueous alteration occurred within the trough.

A number of recent papers have described late occurring aqueous activity elsewhere on Mars. For example, late water-related erosion has been suggested (e.g., Gulick and Baker, 1990; Carr, 1996, 2006; Mangold et al., 2004; Fassett and Head, 2008; Dickson et al., 2009; Fassett et al., 2010) and some events appear approximately contemporary with the formation of the deposits in this Noctis trough.
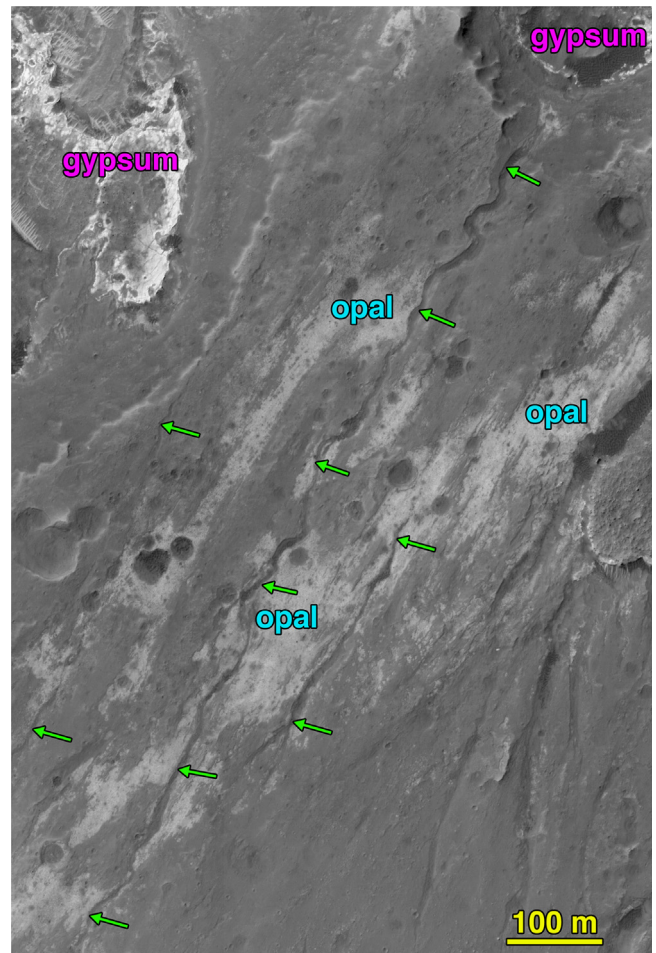
These include valley incision on some Martian volcanoes (Gulick and Baker, 1990; Fassett and Head; 2008), late alluvial fan activity in Margaritifer Terra and elsewhere (Baker and Partridge, 1986; Moore and Howard, 2005; Grant and Wilson, 2011, 2012), a variety of putative supraglacial and proglacial valleys (Fassett et al., 2010), and late geomorphic activity in the Electris region (Grant and Schultz, 1990) that included valley incision (Howard and Moore, 2011). Hence, the Late Hesperian to Amazonian activity in this Noctis trough could reflect synoptic precipitation occurring relatively late in Martian history.

One possible source of water for a late water-driven activity in the trough and elsewhere is water that was debouched into the northern lowlands during late outflow channel formation (e.g., Rotto and Tanaka, 1995; Carr, 2006). Much of this water may have been stored as groundwater prior to outflow activity (e.g., Grant and Parker, 2002) and its release to the surface during outflow channel formation would have reinvigorated a global hydrologic cycle on Mars upon release onto the surface from where it could be redistributed as precipitation in the southern highlands (Luo and Stepinski, 2009).

Under this scenario, synoptic precipitation and any associated runoff would have continued, perhaps accentuated by volcanic activity, topography, and/or orbital variations (e.g., Laskar et al., 2004), until the inventory of water in the northern lowlands was depleted via trapping in the highlands and/or was buried in situ (Mouginot
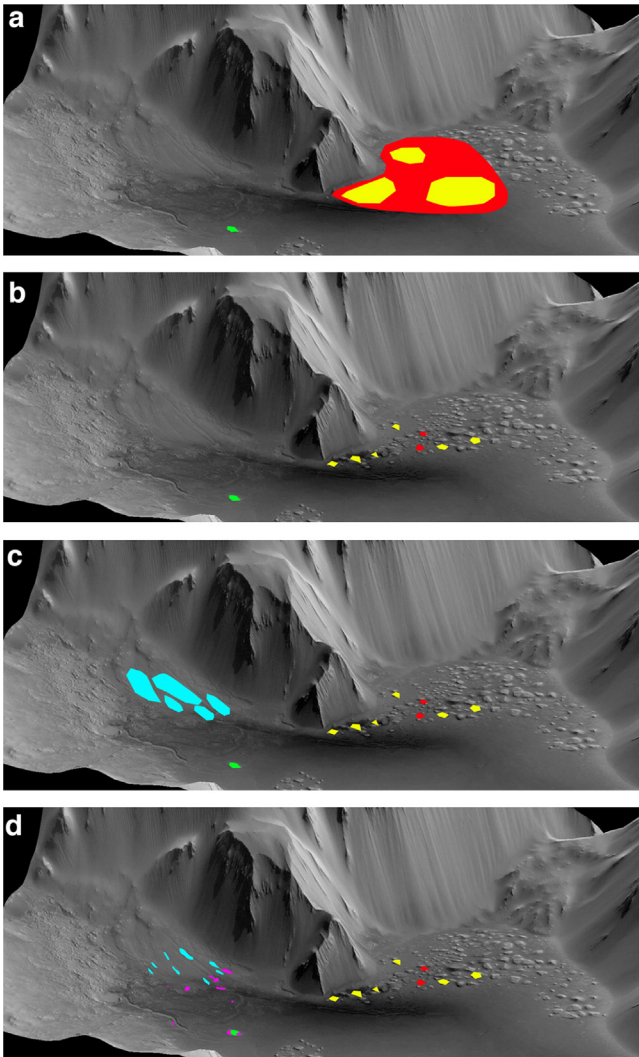
Fig. 16. Proposed sequence of events for the formation of the geologic units and mineral deposits (see text for more details). Colors correspond to the same deposits listed in Fig. 3.

et al., 2012). In the absence of later periods of outflow activity (McEwen et al., 2012) or other means for enabling widespread availability of water at the surface, runoff related to global scale precipitation on Mars likely came to an end.

If our interpretations are correct, then the hydrated materials and fluvial channels in this Noctis trough relate to a late period of widespread, albeit light precipitation. As noted in previous studies (e.g., Grant and Wilson, 2011, 2012) the occurrence of these deposits and associated geomorphic landforms favors precipitation dominated by snowfall and occasional melting that directly enhance the past habitability at the sites at a time in Martian history previously felt to reflect fairly cold, dry, and inhospitable conditions. Limited snowfall could be concentrated in the Noctis trough by winds, thereby producing locally significant accumulations capable of producing runoff upon melting, as hypothesized for alluvial fans in craters elsewhere (Grant and Wilson, 2011, 2012).

Alternatively, these deposits could reflect localized processes within some Noctis depressions, perhaps from hydrothermal activity or snow melt related to events from nearby Tharsis volcanic activity. Two nearby troughs of Noctis contain diverse mineral suites, including mixtures of sulfates, clays, and hydrated silica (Weitz et al., 2011; Thollot et al., 2012), and several other troughs have opal and jarosite (Weitz et al., 2010). Thollot et al. (2012) proposed that basaltic bedrock and volcanic ash deposited

within one Noctis Labyrinthus trough were altered by warm acidic groundwater to produce a progression of mineral phases. Weitz et al. (2011) noted that the deposits within two Noctis troughs both pre- and post-dated depressions within the troughs, indicating multiple episodes of aqueous events. The lack of fluvial features along the adjacent plateaus suggests that the source for the water within these two troughs must have been from groundwater or snow/ice (Weitz et al., 2011), perhaps when water became concentrated within the troughs as windblown accumulations of snow or during periods of high obliquity, as has been suggested for snow/ice in another Noctis trough (Mangold et al., 2010b). Because these other troughs did not exhibit fluvial channels, the trough detailed in this paper appears to represent a unique example of aqueous conditions for this region.

2.4. Sequence of events

Based upon our observations and the stratigraphic relationships, we suggest the following sequence of events to explain the formation of the geologic units and mineral deposits (Fig. 16):

(a) The proto-trough may have been confined to the northern and deepest portion of the current trough. Here, the light-toned layered deposits were emplaced in the Late Hesperian by unknown processes, perhaps as volcanic ash from Tharsis volcanoes (Thollot et al., 2012) or evaporation in a lacustrine environment. Some of these deposits were altered by water to form the Al-clays and hydrated silica. This is likely to have taken place in mildly acidic conditions (e.g. Chamley, 1989). Hydrated silica converts to opal-CT and then to quartz in solution (Siever, 1962) over approximately 100 million years (Tosca and Knoll, 2009). Thus, the presence of opal or some form of hydrated silica implies that water availability after deposition of this silica must have been limited. A bright mound composed of PHS appears to have formed around this time as well, perhaps in association with lower pH water near the central portion of the trough floor, although PHS minerals form under a range of pH conditions and cation concentrations.

(b) Continued collapse and enlargement of the trough disrupted and faulted some of the light-toned layered deposits. Subsequent eruptions along the trough floor during the Late Amazonian (Mangold et al., 2010a) embayed the chaotic terrain and covered much of the light-toned layered deposits. Later erosion of these lava flows in the northwestern portion of the trough enabled some of the light-toned deposits to be exhumed.

(c) In the southern portion of the trough, SLM formed along the wallrock slopes, followed by mass wasting that created unit LB. A lava pit and associated channel then formed in LB and continued to flow down to the trough floor. Opal likely formed at this time by alteration of the upper surfaces of SLM. Melting ice and/or snow created channels and valleys along SLM.

(d) Deposition of gypsum took place and covered portions of LB and SLM, including some of the fluvial channels and the volcanic channel. Gypsum deposition generally prevails over anhydrite for temperatures below 40 °C (e.g. Sievert et al., 2005). YSD formed by unknown processes and covered portions of SLM, LB, and the gypsum. Subsequent erosion of YSD and the opal and gypsum resulted in the distribution we now observe.

3. Conclusions

A depression within Noctis Labyrinthus displays a diversity of deposits and minerals that hold clues to late aqueous alteration environments on Mars that occurred during the otherwise generally drier and colder Late Hesperian to Amazonian.

We identified several episodes of aqueous activity that resulted in both alteration to form hydrated minerals and creation of fluvial channels. In the northern portion of the trough, mixtures of opal and Al-clays underlie younger lava flows. Exposures of numerous interbedded light- and dark-toned layers are consistent with multiple episodes of deposition and/or alteration.

In the southern portion of the trough, gypsum- and opal-bearing materials appear together along lower wallrock slopes in association with channels. The opal-bearing materials are dissected by the channels and valleys while the gypsum-bearing materials fill in the valleys and other depressions. The gypsum-rich and opal-rich materials could have formed under similar mildly acidic, low temperature conditions, with the opaline deposits forming initially during high silica availability in solution, followed by the gypsum deposits during higher Ca availability in solution. Alternatively, the two materials could be unrelated and derived from distinct aqueous sources at different times.

An unusually bright mound in the southeastern portion of the trough displays spectral features consistent with a polyhydrated sulfate while gypsum-bearing materials appear to drape and surround its base. Hence, multiple episodes of aqueous deposition and alteration under changing water chemistry occurred throughout the trough.

The presence of fluvial channels suggests ice and/or snow melt may have sourced some of these channels and the occurrence of the various minerals is consistent with such an origin. It is possible that snow or ice accumulations were the result of synoptic precipitation concentrated in the trough by the wind, similar to what has been hypothesized for late fan formation elsewhere on Mars (Grant and Wilson, 2011, 2012). Consequently, these findings support recent interpretations that a synoptic period of aqueous activity occurred relatively late in Martian history, although favorable localized conditions at Noctis Labyrinthus unrelated to this synoptic precipitation may also explain the hydrated deposits found within this trough and several others. A future rover exploring this region could assess questions related to the geochemical evolution and alteration environment in the Late Hesperian to Amazonian, including the possibility that relatively late occurring habitable settings existed on Mars.

Acknowledgments

References

Anderson, J.H., Wickersheim, K.A., 1964. Near infrared characterization of water and hydroxyl groups on silica surfaces. Surface Science 2, 252–260.

Baker, V.R., Partridge, J.B., 1986. Small Martian valleys: pristine and degraded morphology. Journal of Geophysical Research 91, 3561–3572.

Belousov, A.B., 1995. The Shiveluch volcanic eruption of 12 November 1964—explosive eruption provoked by failure of the edifice. Journal of Volcanology and Geothermal Research 66 (1–4), 357–365.

Bibring, J.-P., Langevin, Y., Mustard, J.F., Poulet, F., Arvidson, R., Gendrin, A., Gondet, B., Mangold, N., Pinet, P., Forget, F., 2006. the OMEGA team, 2006. Global mineralogical and aqueous Mars history derived from OMEGA/Mars Express Data. Science 312, 400–404, http://dx.doi.org/10.1126/science.1122659.

Bishop, J.L., Schiffman, P., Lane, M.D., Dyar, M.D., 2005. Solfataric Alteration in Hawaii as a Mechanism for Formation of the Sulfates Observed on Mars by OMEGA and the MER Instruments, Paper Presented at Lunar Planetary Science XXXVI., Lunar and Planetary Institute, Houston, Abstract #1456.

Bishop, J.L., Lane, M.D., Dyar, M.D., Brown, A.J., 2008. Reflectance and emission spectroscopy study of four groups of phyllosilicates: smectites, kaolinite-serpentines, chlorites and micas. Clay Minerals 43, 35–54.

Bishop, J.L., et al., 2009. Mineralogy of Juventae Chasma: sulfates in the light-toned mounds, mafic minerals in the bedrock, and hydrated silica and hydroxylated ferric sulfate on the plateau. Journal of Geophysical Research 114, E00D09, 10.1029/2009JE003352.

Bishop, J.L., Gates, W.P., Makarewicz, H.D., McKeown, N.K., Hiroi, T., 2011. Reflectance spectroscopy of beidellites and their importance for Mars. Clays and Clay Minerals 59 (4), 376–397.

Bishop, J.L., Rampe, E.B., Bish, D.L., Baker, L.L., Abidin, Z., Matsue, N., Henmi, T., 2013. Spectral and hydration properties of allophane and imogolite. Clays and Clay Minerals 61, 57–74.

Calvert, S.E., 1974. Deposition and diagenesis of silica in marine sediments. In: Hsü, K.J., Jenkyns, H.C. (Eds.), Pelagic Sediments: On Land and under the Sea. Blackwell Scientific, Oxford, pp. 273–299.

Carr, M.H., 1996. Water on Mars. Oxford Univ. Press, New York, NY.

Carr, M.H., 2006. The Surface of Mars. Cambridge Univ. Press, Cambridge, U. K p. 307.

Chamley, H., 1989. Clay Sedimentology. Springer-Verlag, New York p. 623.

Christensen, P.R., Ruff, S.W., 2004. Formation of the hematite-bearing unit in Meridiani Planum: evidence for deposition in standing water. Journal of Geophysical Research 109, E08003, http://dx.doi.org/10.1029/2003JE002233.

Conley, R.F., Bundy, W.M., 1958. Mechanism of gypsification. Geochimica et Cosmochimica Acta 15 (1–2), 57–72.

Dickson, J.L., Fassett, C.I., Head, J.W., 2009. Amazonian-aged fluvial valley systems in a climatic microenvironment on Mars: melting of ice deposits on the interior of Lyot Crater. Geophysical Research Letters 36, L08201.

Elzea, J.M., Odom, I.E., Miles, W.J., 1994. Distinguishing well ordered opal-CT and opal-C from high temperature cristobalite by x-ray diffraction. Analytica Chimica Acta 286 (1), 107–116.

Fassett, C.I., Dickson, J.L., Head, J.W., Levy, J.S., Marchant, D.R., 2010. Supraglacial and proglacial valleys on Amazonian Mars. Icarus 208, 86–100.

Fassett, C.I., Head III, J.W., 2008. The timing of Martian valley network activity: constraints from buffered crater counting. Icarus 195, 61–89.

Fishbaugh, K.E., Poulet, F., Chevrier, V., Langevin, Y., Bibring, J.-P., 2007. On the origin of gypsum in the Mars north polar region. Journal of Geophysical Research 112, E07002, http://dx.doi.org/10.1029/2006JE002862.

Flahaut, J., Quantin, C., Allemand, P., Thomas, P., Le Deit, L., 2010. Identification, distribution and possible origins of sulfates in Capri Chasma (Mars), inferred from CRISM data. Journal of Geophysical Research 115, E11007, http://dx.doi.org/10.1029/2009JE003566.

Gulick, V.C., Baker, V.R., 1990. Origin and evolution of valleys on Martian volcanoes. Journal of Geophysical Research 95, 14,325–14,344, http://dx.doi.org/10.1029/JB095iB09p14325.

Grant, J.A., Schultz, P.H., 1990. Gradational epochs on Mars: evidence from westnorthwest of Isidis Basin and Electris. Icarus 84, 166–195.

Grant, J.A., Parker, T.J., 2002. Drainage evolution in the Margaritifer Sinus region, Mars. Journal of Geophysical Research 107, 5066.

Grant, J.A., Wilson, S.A., 2011. Late alluvial fan formation in southern Margaritifer Terra, Mars. Geophysical Research Letters 38, L08201.

Grant, J.A., et al., 2010. The science process for selecting the landing site for the 2011 Mars Science Laboratory. Planetary and Space Science , http://dx.doi.org/10.1016/j.psss.2010.06.016.

Grant, J.A., Wilson, S.A., 2012. A possible synoptic source of water for alluvial fan formation in southern Margaritifer Terra, Mars. Planetary and Space Science 72, 44–52, 10.1016/j.pss.2012.05.020.

Hardie, L.A., Eugster, H.P., 1971. The depositional environment of marine evaporites: a case for shallow, clastic accumulation. Sedimentology 16 (3–4), 187–220.

Henderson, J.H., Jackson, M.L., Syers, J.K., Clayton, R.N., Rex, R.W., 1971. Cristobalite Authigenic origin in relation to Montmorillonite and Quartz Origin in Bentonites. Clays and Clay Minerals 19 (4), 229–238.

Holland, H.D., 2002. Volcanic gases, black smokers, and the great oxidation event. Geochimica et Cosmochimica Acta 66 (21), 3811–3826.

Howard, A.D., Moore, J.M., 2011. Late Hesperian to early Amazonian midlatitude Martian valleys: evidence from Newton and Gorgonum basins. Journal of Geophysical Research 116, E05003.

Jaumann, R., et al., 2007. The high-resolution stereo camera (HRSC) experiment on Mars Express: instrument aspects and experiment conduct from interplanetary cruise through the nominal mission. Planetary and Space Science 55, 928–952, http://dx.doi.org/10.1016/j.pss.2006.12.003.

Kennedy, B.A., 1990. Surface Mining, 2nd Ed. Port City Press, Baltimore, MD, pp. 172–173.

Kirk, R.L., et al., 2008. Ultrahigh resolution topographic mapping of Mars with MRO HiRISE stereo images: Meter-scale slopes of candidate Phoenix landing sites. Journal of Geophysical Research 113, E00A24, http://dx.doi.org/10.1029/2007JE003000.

Langevin, Y., Poulet, F., Bibring, J.-P., Gondet, B., 2005. Sulphates in the northern region of Mars detected by OMEGA/Mars Express. Science 307, 1584–1586.

Laskar, J., Correia, A.C.M., Gastineau, M., Joutel, F., Levrard, B., Robutel, P., 2004. Long term evolution and chaotic diffusion of the insolation quantities of Mars. Icarus 170, 343–364.

Le Deit, L., Bourgeois, O., Mège, D., Hauber, E., Le Mouélic, S., Massé, M., Jaumann, R., Bibring, J.-P., 2010. Geological history of a layered formation covering the

plateaus around Valles Marineris, Mars. Icarus 208, 684–703, 10.1016/j.icarus. 2010.03.012.

Le Deit, L., Flahaut, J., Quantin, C., Hauber, E., Mège, D., Bourgeois, O., Gurgurewicz, J., Massé, M., Jaumann, R., 2012. Extensive surface pedogenic alteration of the Martian Noachian crust suggested by plateau phyllosilicates around Valles Marineris. Journal of Geophysical Research 117, E00J05 2011JE003983.

Luo, W., Stepinski, T.F., 2009. Computer-generated global map of valley networks on Mars. Journal of Geophysical Research 114, E11010.

Malin, M.C., Bell III, J.F., Cantor, B.A., Caplinger, M.A., Calvin, W.M., Clancy, R.T., Edgett, K.S., Edwards, L., Haberle, R.M., James, P.B., Lee, S.W., Ravine, M.A., Thomas, P.C., Wolff, M.J., 2007. Context Camera investigation on board the Mars Reconnaissance Orbiter. Journal of Geophysical Research 112, E05S04, http://dx. doi.org/10.1029/2006JE002808.

Mangold, N., Quantin, C., Ansan, V., Delacourt, C., Allemand, P., 2004. Evidence for precipitation on Mars from dendritic Valleys in the Valles Marineris Area. Science 305, 78–81.

Mangold, N., 2010a. Mineralogy of recent volcanic plains in the Tharsis region, Mars, and implications for platy-ridged flow composition. Earth and Planetary Science Letters 294 (3–4), 440–450, http://dx.doi.org/10.1016/j.epsl.2009.07.036.

Mangold, N., Roach, L., Milliken, R., Le Mouélic, S., Ansan, V., Bibring, J.-P., Masson, P., Mustard, J.F., Murchie, S., Neukum, G., 2010b. A Late Amazonian alteration layer related to local volcanism on Mars. Icarus, 207; b, pp. 265–276, http://dx. doi.org/10.1016/j.icarus.2009.10.015.

Masse, M., Bourgeois, O., Le Mouelic, S., Verpoorter, C., Le Deit, L., Bibring, J.P., 2011. Martian polar and circum-polar sulfate-bearing deposits: sublimation tills derived from the North Polar Cap. Icarus 209, 434–451, http://dx.doi.org/ 10.1016/j.icarus.2010.04.017.

McEwen, A., 1989. Mobility of large rock avalanches: evidence from Valles Marineris, Mars. Geology 17, 1111–1114.

McEwen, A.S., Keszthelyi, L.P., Grant, J.A., 2012. Have there been Large, Recent Water Floods on Mars? Lunar and Planetary Science XLIII. Houston, TX, abstract 1612.

McEwen, A.S., Eliason, E.M., Bergstrom, J.W., Bridges, N.T., Hansen, C.J., Delamere, W.A., Grant, J.A., Gulick, V.C., Herkenhoff, K.E., Keszthelyi, L., Kirk, R.L., Mellon, M.T., Squyres, S.W., Thomas, N., Weitz, C.M., 2007. Mars Reconnaissance Orbiter's High Resolution Imaging Science Experiment (HiRISE). Journal of Geophysical Research 112, E05S02, http://dx.doi.org/10.1029/2005JE002605.

McKeown, N.K., et al., 2011. Interpretation of reflectance spectra of mixtures of clay mineral-silica mixtures: implications for Martian clay mineralogy at Mawrth Vallis. Clays and Clay Minerals 59 (4), 400–415.

McLennan, S.M., 2003. Sedimentary silica on Mars. Geology 31, 315–318, 10.1130/ 0091-7613(2003)031.

Mège, D., Cook, A.C., Garel, E., Lagabrielle, Y., Cormier, M., 2003. Volcanic rifting at Martian grabens. Journal of Geophysical Research 108 (E5), 5044, http://dx.doi. org/10.1029/2002JE001852.

Milliken, R.E, Swayze, G.A., Arvidson, R.E., Bishop, J.L., Clark, R.N., Ehlmann, B.L., Green, R.O., Grotzinger, J.P., Morris, R.V., Murchie, S.L., Mustard, J.F., Weitz, C., 2008. Opaline silica in young deposits on Mars. Geology 36, 847–7580, http: //dx.doi.org/10.1130/G24967A.1.

Moore, J.M., Howard, A.D., 2005. Large alluvial fans on Mars. Journal of Geophysical Research 110, E04005.

Morris, R.V., 2000. 11 colleagues, 2000. Mineralogy, composition, and alteration of Mars Pathfinder rocks and soils: evidence from multispectral, elemental, and magnetic data on terrestrial analogue, SNC meteorite, and Pathfinder samples. Journal of Geophysical Research 105, 1757–1817, http://dx.doi.org/10.1029/ 1999JE001059.

Mouginot, J., Pommerol, A., Beck, P., Kofman, W., Clifford, S.M., 2012. Dielectric map of the Martian northern hemisphere and the nature of plain filling materials. Geophysical Research Letters 39, L02202.

Murchie, S., Arvidson, R., Bedini, P., Beisser, K., Bibring, J.-P., Bishop, J., Boldt, J., Cavender, P., Choo, T., Clancy, R.T., Darlington, E.H., Des Marais, D., Espiritu, R., Fort, D., Green, R., Guinness, E., Hayes, J., Hash, C., Heffernan, K., Hemmler, J., Heyler, G., Humm, D., Hutcheson, J., Izenberg, N., Lee, R., Lees, J., Lohr, D., Malaret, E., Martin, T., McGovern, J.A., McGuire, P., Morris, R., Mustard, J., Pelkey, S., Rhodes, E., Robinson, M., Roush, T., Schaefer, E., Seagrave, G., Seelos, F., Silverglate, P., Slavney, S., Smith, M., Shyong, W.-J., Strohbehn, K., Taylor, H., Thompson, P., Tossman, B., Wirzburger, M., Wolff, M., 2007. Compact Reconnaissance Imaging Spectrometer for Mars (CRISM) on Mars Reconnaissance Orbiter (MRO). Journal of Geophysical Research, 112; p. E05S03, http://dx.doi.org/10.1029/2006JE002682.

Murchie, S.L., et al., 2009a. Compact Reconnaissance Imaging Spectrometer for Mars investigation and data set from the Mars Reconnaissance Orbiter's primary science phase. Journal of Geophysical Research 114, E00D07, http: //dx.doi.org/10.1029/2009JE003344.

Murchie, S.L., et al., 2009b. A synthesis of Martian aqueous mineralogy after 1 Mars year of observations from the Mars Reconnaissance Orbiter. Journal of Geophysical Research 114, E00D06, http://dx.doi.org/10.1029/2009JE003342.

Murchie, S., et al., 2009c. Evidence for the origin of layered deposits in Candor Chasma, Mars, from mineral composition and hydrologic modeling. Journal of Geophysical Research 114, E00D05, http://dx.doi.org/10.1029/2009JE003343.

Okubo, C.H., Lewis, K.W., McEwen, A.S., Kirk, R.L., 2008. Relative age of interior layered deposits in southwest Cando Chasma based on high-resolution structural mapping. Journal of Geophysical Research 113, E12002, http://dx.doi.org/ 10.1020/2008JE003181.

Pelkey, S.M., et al., 2007. CRISM multispectral summary products: parameterizing mineral diversity on Mars from reflectance. Journal of Geophysical Research 112, E08S14, http://dx.doi.org/10.1029/2006JE002831.

Prothero, D.R., Schwab, F., 2004. Sedimentary Geology. An Introduction to Sedimentary Rocks and Stratigraphy, 2nd ed. W. H. Freeman and Co., New York.

Quantin, C., Allemand, P., Delacourt, C., 2004. Morphology and geometry of Valles Marineris landslides. Planetary and Space Science 52, 1011–1022.

Rice, M.S., et al., 2010. Silica-rich deposits and hydrated minerals at Gusev Crater, Mars: Vis-NIR spectral characterization and regional mapping. Icarus, 205; , pp. 375–395.

Rotto, S., Tanaka, K.L., 1995. Geologic/geomorphic map of the Chryse Planitia region of Mars. Miscellaneous Investigations Series Map I-2441, U.S. Geological Survey.

Ruff, S.W., et al., 2011. Characteristics, distribution, origin, and significance of opaline silica observed by the Spirit rover in Gusev crater, Mars. Journal of Geophysical Research 116, E00F23, http://dx.doi.org/10.1029/2010JE003767.

Scott, D.H., Tanaka, K.L., 1986. Geologic map of the Western Equatorial Region of Mars. US Geol. Surv. Misc. Invest. Ser., Map, I-1802-A.

Seelos, F.P., 2011. CRISM Data Processing and Analysis Products Update—Calibration, 1076 Correction, and Visualization. 42nd Lunar and Planetary Science Conference, Abstract 1438.

Siever, J., 1962. Silica solubility 0–200 °C, and the diagenesis of siliceous sediments. Journal of Geology 70, 127–150.

Sievert, T., Wolter, A., Singh, N.B., 2005. Hydration of anhydrite of gypsum (CaSO4. II) in a ball mill. Cement and Concrete Research 35 (4), 623–630.

Skok, J.R., Mustard, J.F., Ehlmann, B.L., Milliken, R.E., Murchie, S.L., 2010. Silica deposits in the Nili Patera caldera on the Syrtis Major volcanic complex on Mars. Nature Geoscience 3, 838–841, http://dx.doi.org/10.1038/ngeo990.

Squyres, S., 2006. Mineralogy of the light-toned outcrop rock at Meridiani Planum as seen by the miniature Thermal Emission Spectrometer and implications for its formation. Journal of Geophysical Research 111, E12S03, http://dx.doi.org/ 10.1026/2005HE002672.

Squyres, S.W., et al., 2008. Detection of silica-rich deposits on Mars. Science 320, 1063–1067, http://dx.doi.org/10.1126/science.1155429.

Squyres, S.W., 2012. Initial Opportunity Rover Results at Endeavour Crater, Mars. 43 LPSC 43, Abstract 1892.

Szuimula, I., Bishop, J.L., Fenton, L.K., Brown, A.J., 2013. Composition and Morphology of Gypsum Dunes in Olympia Undae on Mars. LPSC 44, Abstract 2123.

Tanaka, K.L., Davis, P.A., 1988. Tectonic history of the Syria Planum Province of Mars. Journal of Geophysical Research 93 (B12), 14,893–14,917, http://dx.doi.org/ 10.1029/JB093iB12p14893.

Thollot, P., Mangold, N., Ansan, V., Le Mouélic, S., Milliken, R.E., Bishop, J.L., Weitz, C.M., Roach, L.H., Mustard, J.F., Murchie, S.L., 2012. Most Mars minerals in a nutshell: various alteration phases formed in a single environment in Noctis Labyrinthus. Journal of Geophysical Research 117, E00J06, http://dx.doi.org/ 10.1029/2011JE004028.

Tosca, N.J., Knoll, A.H., 2009. Juvenile chemical sediments and the long term persistence of water at the surface of Mars. EPSL 286, 379–386, http://dx.doi. org/10.1016/j.epsl.2009.07.004.

Vaniman, D.T., Bish, D.L., Chipera, S.J., 2008. Calcium Sulfate Hydration, Stability and Transformation on Mars, LPSC XXXIX, Abstract 1816.

Weitz, C.M., Bishop, J.L., 2011. A Proposed Future Mars Landing Site in Noctis Labyrinthus, Lunar and Planetary Science Conference, XXXXII, Abstract 1874.

Weitz, C.M., Milliken, R.E., Grant, J.A., McEwen, A.S., Williams, R.M.E., Bishop, J.L., Thompson, B.J., 2010. Mars Reconnaissance Orbiter observations of light-toned layered deposits and associated fluvial landforms on the plateaus adjacent to Valles Marineris. Icarus 205 (1), 73–102, http://dx.doi.org/10.1016/j.icarus. 2009.04.017.

Weitz, C.M., Bishop, J.L., Thollot, P., Mangold, N., Roach, L.H., 2011. Diverse mineralogy in two troughs of Noctis Labyrinthus, Mars. Geology 39, 899–902, http://dx.doi.org/10.1130/G32045.1.

Weitz, C.M., Noe-Dobrea, E.Z., Lane, M.D., Knudson, A., 2012. Geologic relationships between gray hematite, sulfates, and clays in Capri Chasma. Journal of Geophysical Research 117, E00J09, 10.1029/2012JE004092.

Weitz, C.M., Noe Dobrea, E., Wray, J.J., 2013. Gypsum, Jarosite, and other Minerals Associated with a Blocky Deposit in Western Melas Chasma, 44th LPSC, Abstract 2076.

White, W.B., White, E.L., 2003. Gypsum wedging and cavern breakdown: studies in the Mammoth cave system, Kentucky. Journal of Cave and Karst Studies 65, 43–52.

Williams, L.A., Parks, G.A., Crerar, D.A., 1985. Silica diagenesis, I. Solubility controls. Journal Sedimentary Petrology 55, 301–311.

Wray, J.J., et al., 2011. Columbus crater and other possible groundwaterfed paleolakes of Terra Sirenum, Mars. Journal of Geophysical Research 116, E01001, http://dx.doi.org/10.1029/2010JE003694.

Wray, J.J., Squyres, S.W., Roach, L.H., Bishop, J.L., Mustard, J.F., Noe Dobrea, E.Z., 2010. Identification of the Ca-sulfate bassanite in Mawrth Vallis, Mars. Icarus 209, 416–421, http://dx.doi.org/10.1016/j.icarus.2010.06.001.

Yen, A.S., et al., 2008. Hydrothermal processes at Gusev Crater: an evaluation of Paso Robles class soils. Journal of Geophysical Research 113, E06S10, http://dx. doi.org/10.1029/2007JE002978.

Zuber, M.T., Smith, D.E., Head, J.W., Muhleman, D.O., Solomon, S.C., Garvin, J.B., Abshire, J.B., Bufton, J.L., 1992. The Mars Observer Laser Altimeter Investigation. Journal of Geophysical Research 97, 7781–7797.